TRG

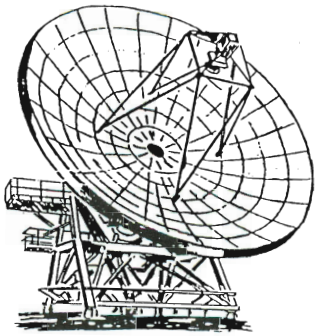

The JCMT - UKIRT NEWSLETTER

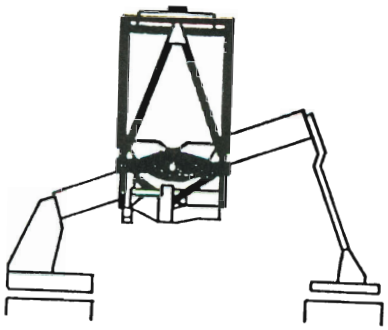

Kūlia I Ka Nu'U

Number 2 August 1991

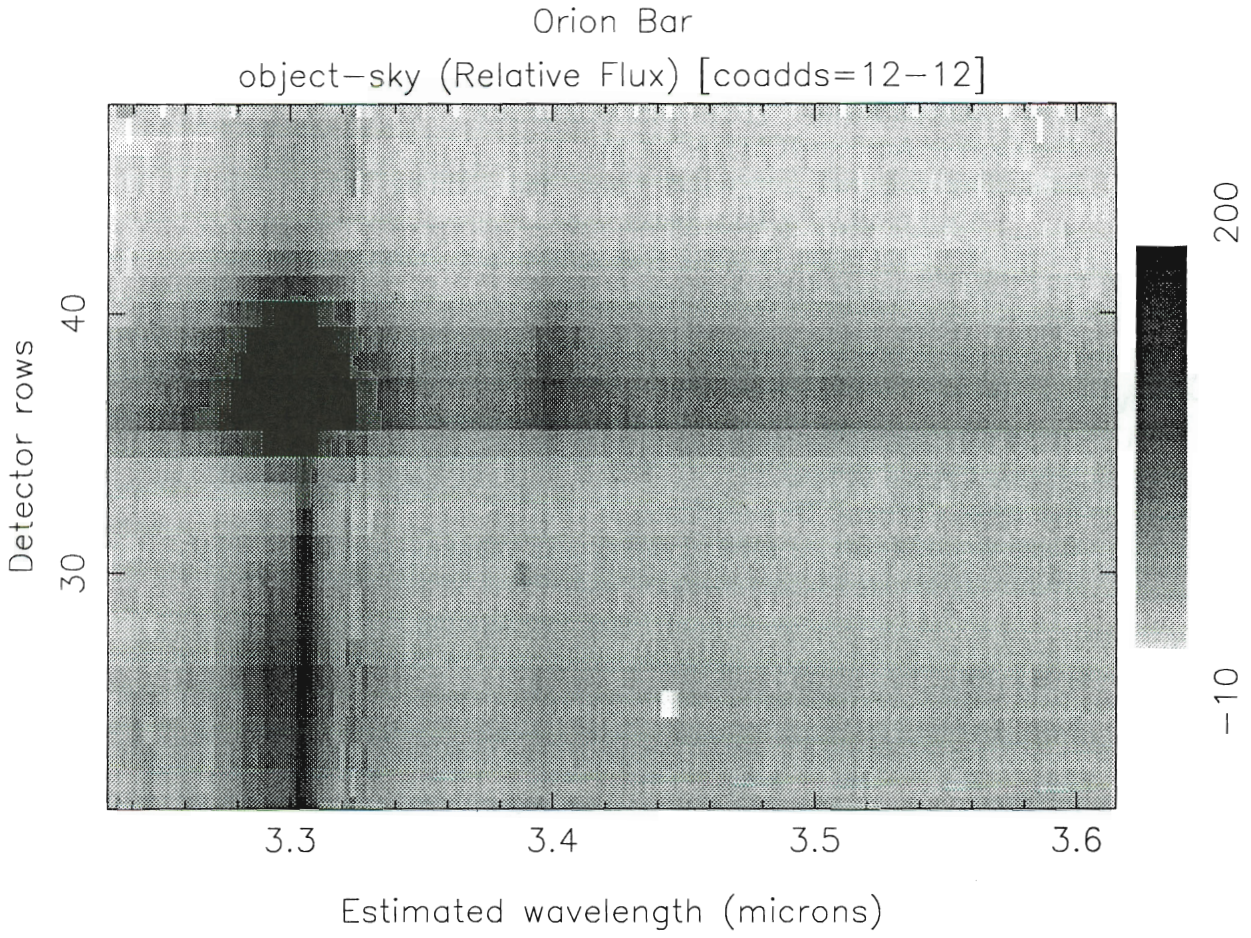

Contents

Cover picture:
One of the first observations made by the new long-slit 1-5μm spectrometer, CGS4, during commissioning on UKIRT on 23 February 1991. The 90 arcsec slit was placed across the ionization in front of the Orion nebula. Note the unresolved hydrogen recombination line Pf-δ (9→5, near 3.3μm) extending to the sharp edge of the "bar", which runs roughly across the middle of this image, and the broader 3.3μm and 3.4μm emission features from small grains/PAHs visible just outside the HII region in the photo-dissociation zone.
CGS4 team

Availability of UKIRT instruments during Semester V (February - July 1992)

UKT6 single channel 1-5μm photometer, 2.3-4.6μm CVF

UKT8 single channel L', N, Q and narrow band 10μm photometer

UKT9 single channel 1-5μm photometer, 1.35-2.6μm CVF

UKT10 2-banger; J or H, and fixed K filter

UKT16 8-banger; N, Q, 30μm and narrow band 10μm

CGS3 8-22μm grating spectrometer, 1x32 channels, resolving powers of ~6 or 200 at 10μm and ~75 at 20 μm. Beam sizes from 1" to 9" diameter.

CGS3 and IRCAM both use the north port of ISU2, and thus are mutually exclusive.

CGS4 1-5μm 58x62 array; echelle, 75 l/mm,and 150 l/mm gratings; long and short focal length cameras (the long focal length camera effectively doubles the resolution of a given grating and halves the pixel size, from 3.6" to 1.8"), and polarimeter.

After an initial commissioning period, extending through Semester U, it is expected that CGS4 will be available for full scientific use in Semester V in all of the above modes, with the possible exception of the long focus camera. However, the status of CGS4 will not be certain until the time of the next PATT meeting, when the commissioning phase is further along. Potential applicants for CGS4 programs should note any future updates on CGS4 performance and availability, in particular for the 300mm camera. (See also page 8, CGS 4 in VAXnotes)

There are many combinations of gratings and camera focal lengths in CGS4. The need to minimize the number of changeovers, which require considerable effort and at least one week of down time, means that some configurations may be avoided during certain semesters, while others may be scheduled during limited periods (at some inconvenience to some observers). If more than one CGS4 configuration is acceptable to the applicant, he/she should indicate this on the proposal.

Unless there are unscheduled long down times for CGS4, **CGS2** (the 7 channel, 1.0-5.4μm grating spectrometer) and the 3-5μm FPs will not be available during Semester V.

IRCAM 58x62 array, 1-5μm photometric and various narrow band filters;
0.6" per pixel (36" field of view); 1.2" per pixel (72"field of view); 0.3" per pixel available using ambient temperature 2X magnifier. **Note:** due to availability of only one IRCAM, 2.4" pixel scale will **not** be offered.

IRPOL 1-5μm polarimeter for IRCAM, UKT6, UKT9, and CGS4. Note that the unvignetted field of view of IRCAM through IRPOL is ~35"; hence optimal usage of IRCAM+IRPOL is with 0.6" pixels.

CORONAGRAPH A coronagraph for use with IRCAM is available, subject to the agreement of, and collaboration with, Dr. Ben Zuckerman of UCLA, who is its owner. Applicants should discuss any such proposals with Dr. Zuckerman before submission of the application.

FABRY PEROT's 2μm: 12, 25, 90 and 300 km/s resolutions; can be used with IRCAM and with UKT9; unvignetted field of view through IRCAM is ~ 60".

VISPHOT single channel visible B or V band photometer, can be operated simultaneously with any of the above single channel instruments and with UKT10.

Tom Geballe
Associate Director UKIRT
JAC

CGS3 Comes of Age

CGS3 is UKIRT's common-user 10-20 micron spectrometer. It is a liquid helium - cooled, low resolution grating spectrometer employing a 1 x 32 array of Si:As detectors. Three gratings allow 10 and 20μm spectroscopy, with two choices of resolution in the 10 micron window.

The instrument was built at University College London. Following tests at ROE, it was successfully commissioned last summer at UKIRT. However, CGS3 encountered severe difficulties last semester, particularly involving communications between its Sinclair microcomputer and the summit Vax cluster. Fortunately, only one group of observers was assigned CGS3 time last semester and had to endure the problems. This spring, following installation of CGS4, considerable time was devoted to "cleaning up" CGS3's electronics. This work was done in Hilo, mainly by Joanne Griffin and Tim Chuter. Following their work and three nights of engineering, three research groups successfully used CGS3 in May. In addition, CGS3 was used for Service observing for the first time, and the instrument filled in admirably for CGS4 in late May.

A few problems with the operation of CGS3 still remain, but cause only a small amount of lost time. The worst of these, involving driving from one grating to another, should be solved by next semester. CGS3's software, although easy to use and already improved somewhat by Alan Bridger during the engineering nights, is in need of a number of enhancements, as is CGS3's data reduction program. Work on some of these software projects is proceeding; additional work probably will be initiated after several CGS4-related software improvements are complete.

The table below summarizes CGS3's performance and the figures show several recent spectra obtained with the low resolution 10 micron grating (spectra have been obtained successfully with the other gratings as well). Both a CGS3 manual and a document describing data reduction now exist in INFORM.

Tom Geballe
JAC

[Please note: the flux densities given on the vertical axes of the figures are in error; they should be 10^8x smaller than shown! - Ed.]

TABLE 1

Grating Name ruling	Available Wavelengths μm	Spectral range μm	Optimum Filter	Average Detector spacing μm	Resolution FWHM μm	Sensitivity 1σ 1sec		
						mag	Jy	flux E^{-14} W/m2
HIRES_10 105 l/mm	7-15	1.6	7-22	0.052	0.060	2.3	5.0	0.8
LORES_10 35 1/mm	7-15	5.8	7-22	0.19	0.20	3.0	2.5	1.5
20 25 l/mm	16-24	8.3	15-24	0.27	0.275	1.7	2.1	0.5

Measurements made in the 5" aperture. Spectral profile is roughly rectangular.

Figure 1.
A spectrum of Nova Her, obtained by Tom Geballe and Suzie Ramsay. A strong and broad dust emission feature can be seen (see also IAU Circular No. 5273). The minor sub-feature at 9.5μm may be an artifact of the strong telluric ozone absorption at that wavelength. Total integration time was 4 minutes.

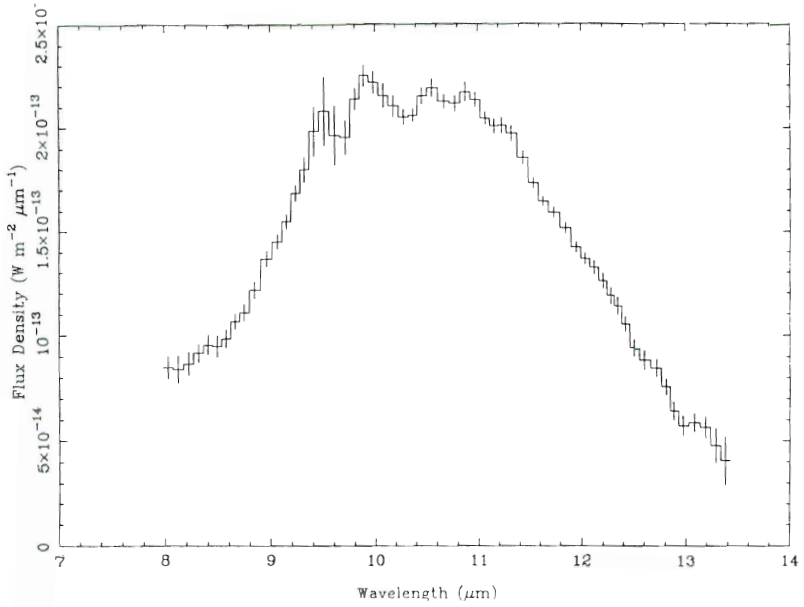

Figure 2.
A low resolution spectrum of Source 'a' in GGD27-IRS obtained by Colin Aspin. GGD27-IRS is an active region of high mass star formation containing a CO outflow, several bright near-infrared sources and extensive near-infrared reflection nebulosity. The Sources 'a' and 'b' in GGD27-IRS (see Aspin et al., 1991 in press) was found to show 3.3 μm 'PAH' emission features. The 10 μm spectrum shows several bands of 'PAH' emission (7.7, 8.6, 11.3, 12.6 μm). Source 'a' has an N magnitude of ~3.2; this spectrum was obtained in a total integration time of ~200 seconds.

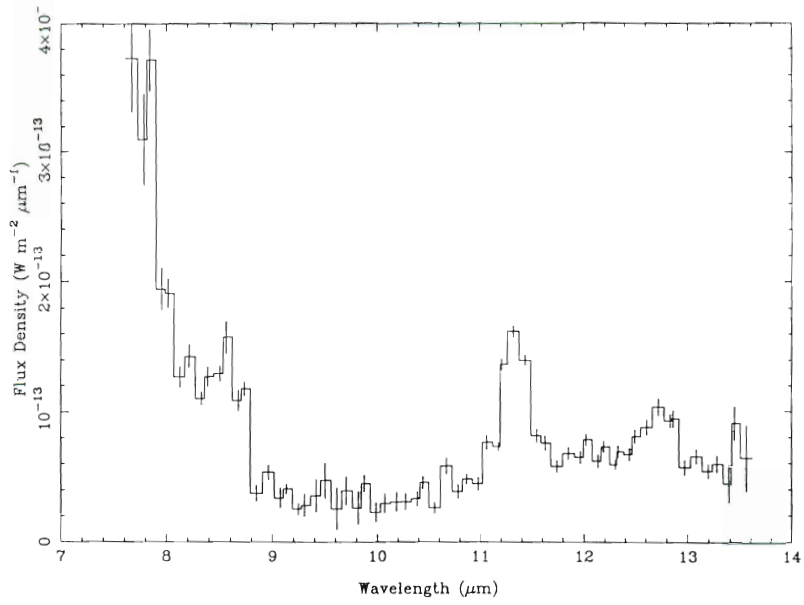

Figure 3.
A 10 μm low resolution spectrum of W51-IRS1N also taken by Colin Aspin. W51 is a compact HII region containing several infrared sources; IRS1N is a nebulous region close to the more compact IRS1S. IRS1N shows a rising red continuum with emission lines of S IV (10.51μm) and Ne II (12.81μm) and a possible detection of Ar III (8.99μm). There is also a faint 11.3μm 'PAH' emission feature. This spectrum was acquired in ~100 seconds.

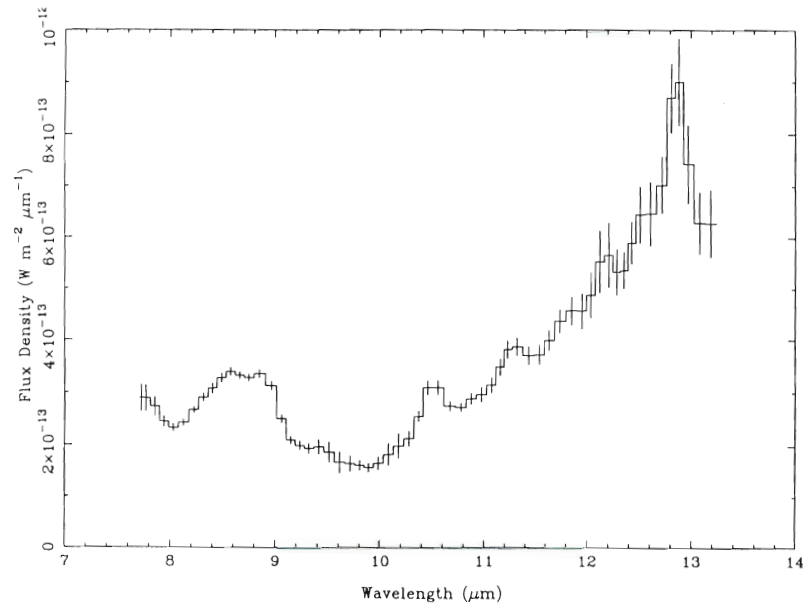

IRCAM Update

Ghost Reflections in IRCAM

During the May engineering period, considerable progress was made in eliminating internal in-focus reflections in IRCAM. The normal flat window has been replaced with a zero power meniscus, and spacers have been made to tilt the filters and throw any reflections well off the array. Unfortunately, tilts of the narrow-band filters would result in significant wavelength shifts, so only broadband filters will be tilted. Users should find that broadband filters no longer have ghosts while the ghosting in the narrowband filters has been reduced by about 50%.

Using the x2 Magnifier with 1.2" Pixel Scale

Tests were conducted to see the usefulness of using the warm x2 magnifier (designed for use with 0.6" pixels) with the 1.2" pixel scale. Results are as follows:

resulting pixel scale	0.60 "/pixel
field distortion	negligible
vignetting	none
background level	about 3-4 times that achieved when using the cold internal lens to get 0.6" pixels.

The conclusion is that the magnifier will work quite well with the 1.2" pixels but does result in a S/N loss of 1.7 to 2 in background limited applications. It therefore may be useful for observers who mainly require 1.2" pixels, but want a few frames of an object at higher resolution during their run.

The Institute for Astronomy K' Filter

An IFA K' filter has been installed in IRCAM. This filter, which has half maxima at 1.95 and 2.3 microns thus missing the thermal end of the K window, has a nominal background level 2.5 times lower and a throughput about 10% lower than a normal K filter. It should thus offer a 40% improvement in S/N for background limited applications. Unfortunately, the blocking filter we use with the K' reduces throughput by a further 25%, so the S/N is only slightly improved over normal K. Further experiments are planned with a different blocker. The K' filter will be available for the next semester.

IRCAM Starlink Software

A new release of the Starlink data reduction package is currently being prepared. This will soon be sent to ROE and from there it can be accessed by any Starlink site and copied to the 'local' node. The new release contains the relevant software to drive a Vaxstation running DecWindows. It also includes additional documentation on using IRCAM (the IRCAM operations manual) and some files describing the main reduction programs (e.g. MED3D, DARKLOT etc). Included in the release is a DCL program called PREDICT. This will allow users to obtain estimates of the S/N obtainable using IRCAM for specific exposure times, number of coadds, number of separate images combined to a final image and flux (in DN) per coadd; the latter value can be obtained from the IRCAM operations manual appendix.

IRCAM Data Acquisition Software

The IRCAM data acquisition and instrument control software continues to evolve with time. An additional command called SETUP is now available which presents the user with a menu of items to change. These items include the exposure time, number of coadds, number of images taken, the filter and the object name.

Future Plans

At a date yet to be decided, we anticipate upgrading the IRCAM instrument control and data acquisition system to use that provided to run our new 2D spectrometer, CGS4. This system is considerably more flexible than the current IRCAM system and includes options such as observation queuing, automatic on-line data reduction, etc. It is thought that use of the CGS4 system will considerably enhance the operational performance and efficiency of IRCAM and make running our two array instruments virtually identical.

Mark Casali
Colin Aspin
JAC

Remote Observing with UKIRT

Remote observing with UKIRT has been available since late March, when the installation and testing of the dedicated line from the UK to Hawaii was finished. All UKIRT instruments except CGS4 may be used. Images from the UKIRT acquisition TV are presently unavailable because of technical problems but could become available again at short notice - please ask for the latest information.

The remote observing system is very easy to use. A remote observer (RO) logs on to one of the remote-observing usernames at UKIRT and selects from a menu which of the observing screens he/she wants to see. Usually the RO has a separate login for each screen, although it is also possible to swap between screens from a single login. There are mechanisms for file transfers and for communications with people at the telescope.

There are two possibilities for remote observing with UKIRT: passive observing and active observing. With passive observing the RO watches progress at the telescope but does not control any of the observations. However, with active observing the RO can watch progress and control the observations. Authorisation is needed for both passive and active observing, and active observing will certainly be more restricted.

Copies of the draft manual for remote observing are available on request.

The 56 kbit/sec dedicated line from the UK to Hawaii is available from Starlink and Janet nodes throughout the UK and not just ROE. It has been generally reliable, although there have been occasional breakdowns. From about mid-July, following the delivery of some hardware, two compressed voice channels from ROE to JACH, UKIRT and JCMT will also operate across the line. These channels should be accessible to remote observers at sites other than ROE for the cost of a normal phone call to ROE.

With SERC funding restricted to one observer in most cases, this is certainly a good time for UK astronomers to consider remote observing. Remote observers can undoubtedly take a very important part in observations - watching progress and advising (with sea-level oxygen); reducing data as they are taken and assessing their quality; preparing forthcoming observations; supervising students and supervising supervisors; and so on. Experienced observers may also request authorisation from the telescope staff to control the instruments remotely.

Potential remote observers should contact me in the first instance for further details. I will then contact the astronomer-in-charge at the telescope and the assigned support astronomer, as appropriate, for discussions about feasibility and for authorisation.

Roger Clowes

Starlink: REVAD::RGC
Janet: RGC @ UK.AC.ROE.STARLINK
SPAN: 19527::REVAD::RGC
Internet: RGC @ STARLINK.ROE.AC.UK

Comment on proposals submitted for Semester U

It is well known that the pressure for observing time on the UKIRT is high. One factor that the committee must take into account in assessing the relative merits of the applications is the suitability of available instrumentation for the proposed observations. Last semester a number of applications requesting the use of IRCAM required the combination of a number of frames to cover the necessary field of view. A moderate amount of so-called mosaicing of IRCAM images is acceptable, but applicants should be aware that large format infrared arrays are now available on a number of other (non-UK) telescopes, and the AAT (IRIS), to which UK astronomers can apply. On grounds of efficient use of telescope time it is therefore difficult to justify awarding time on the UKIRT for such proposals, bearing in mind the competition from applications that do not require multiple imaging, and those requesting spectroscopic time. IRCAM continues to be a very powerful instrument for many projects, and we look forward to the introduction of large format arrays into UKIRT instrumentation as soon as is practicable.

Martin Ward
UKIRT TAG Chairman

The M and narrow-band M filters in UKT9

UKT9 possesses two filters in the M (4.5-5.0μm) band. One of these is the "standard" M filter, which has a central wavelength of 4.7μm and a bandwidth of 14 percent. Because of the high background near 4.7μm, in UKT9 this filter can only be used in apertures less than or equal to 5". (In UKT6, which has a smaller low feedback resistor, it can be used in the 7.8 arcsec aperture.) At UKIRT, short wavelength photometry normally is done in apertures larger than 5" for reasons of photometric accuracy. When UKT9 is being used and M-band photometry is also required, considerable time is lost in switching apertures, peaking up, etc.

Because of the above inefficiency and the general "dirtiness" of the M window (and consequent uncertain airmass correction), it was decided a few years ago to purchase a narrow band filter, which would be centered in the cleanest portion of the M band. The filter that was purchased and is installed in UKT9 has a central wavelength of 4.64μm and a bandwidth of 3.5 percent, and is known as nbM. It can be used with UKT9's 7.8" aperture.

The relationship of the M and nbM filters in UKT9 was tested by obtaining photometry of bright stars of various spectral types, using the 5 arcsecond aperture on a night of good seeing. The results show that there is a constant (to within one percent) ratio of signal for spectral types earlier than K, and hence that the nbM photometry may be used to infer accurate M band magnitudes for such stars. At spectral types K and later, the uneven distribution of photospheric CO absorption lines in the M band would be expected to cause differences of a few percent in the behaviour of the two filters.

Because of the greater efficiency in using nbM, M band photometry done by staff members using UKT9 normally will be done using the nbM filter, unless there are specific instructions (e.g., by the Service applicant) to use the "standard" M filter. In other words, a request for M photometry may be treated as a request for nbM photometry, unless the requester explicitly states that the "standard M filter" must be used.

Tom Geballe
JAC

Filter profile data - errata

A UKIRT user has kindly pointed out some errata in the article 'Transmission Profiles for Filters in UKIRT Instrumentation' in the March 1991 Newsletter (page 4).

(i) the NBLFILT.DAT file, labelled as L filter (3.406μm) contains the correct filter profile, but this peaks at 3.589μm, not 3.406μm.

(ii) I234FILT.DAT described a filter peaking at 2.32μm, not 2.34μm. This file has been renamed to I232FILT.dat.

(iii) Similarly, the I308FILT.DAT profile peaks at 3.10μm and has been renamed I310FILT.DAT.

(iv) Files I206FILT.DAT, I221FILT.DAT and I340FILT.DAT are missing. We are attempting to find the manufacturer's profiles for these filters, but so far unsuccessfully.

Andy Longmore
ROE

UKIRT Time in Semester U

The July PATT meeting considered 119 UKIRT proposals for Semester U, and awarded time to 36 of them. The time applied for was 4 times the time available, and for CGS4 the oversubscription rate was 4.3x.

UKIRT Service Observing

Just a reminder that the UKIRT service observing programme provides the opportunity to have short (about 2 hour) observations made on your behalf by UKIRT staff astronomers. If you are not familiar with the programme then either read the appropriate section in the UKIRTINFORM system, or read the files DISK$USER3:[UKIRTSERV]UKIRTSERV.OBS and [UKIRTSERV]UKIRTSERV.HOW on the ROE STARLINK VAX or e-mail your questions to UKIRTSERV at ROE. If you would like to be put on our mailing list and receive details of schedules, deadlines and instrument availability send your e-mail address to UKIRTSERV on the ROE STARLINK VAX (UK.AC.ROE. STAR).

Please remember to tell us if you complete your observation during a normal PATT run, or wish to withdraw it for other reasons, so we can delete it from our target list. We also would be pleased to know when and where you publish your data, so we can keep our files up to date.

Results from the Survey

Many users will know that a survey of Service Observing was carried out last year. This showed that for the periods June 1988 to May 1990 180 proposals were received and 110 were attempted. UK applications came from 19 different institutions.

The survey showed that most users were able to contact UKIRTSERV easily, had received their data promptly and were able to reduce it satisfactorily. Ten papers arising from these data had appeared in, or were in press for, refereed journals. This result was independently confirmed when eight papers involving service data were found in the 1990 UKIRT publications list.

About half the users who had not published their data referred to papers in preparation; we await these with interest. Of the remainder, a significant fraction were feasibility studies for PATT proposals.

The service team is encouraged by these results, which confirm the wide user community and productivity of the programme. In particular its value for transient events has again been shown by successful observations of comets and for observations in conjunction with other ground and space based programmes. As always, we remain receptive to advice, criticism and enquiries from new users.

Schedule for Semester U

This is not available as we go to press; users on our e-mail circulation will receive information on deadlines in the usual way.

Report on Semester T

Ten nights were scheduled for service in Semester T, and at the time of writing only 6 have taken place. The remainder will occur while the Newsletter is 'in press'. Since the last report, 21 applications have been received. These were graded as follows: 7 A, 12 AB, 1 B and one reject.

Following the dismal weather in the end of Semester S we had hopes of better things, but these were not initially forthcoming as the first two nights in March were lost due to high winds. However the third night in March was clear and some of the lost time was recovered in later AIC and engineering nights during March and April. Conditions on May 25 were excellent.

A total of 28 programmes were attempted, of which two were ongoing monitoring, 19 were completed and 7 were partly completed.

With only a few nights so far it may be premature to attempt to summarise highlights, but service data was included in the follow-up observations of the IRAS galaxy at z=2.286 reported by Rowan Robinson *et al.* in 'Nature'. During the March service run and subsequent discretionary time J, H, K IRCAM images were obtained for Dr Gerry Skinner of Birmingham University. These covered the error circles determined with the TTM coded mask X-ray telescope on the MIR space station for several X-ray and gamma-ray sources in the galactic centre and galactic bulge. Of prime importance is 1E1740.7-2942, the hard X-ray source ~ 1^{o} from the galactic nucleus which seems to have exhibited a gamma-ray outburst indicating electron-positron annihilation. Dr Skinner has reported that the field is crowded, with several candidate objects within the 12 arcsec error circle, but the service results imply little or no emission at the position of a radio-source which has since been detected within the circle. This has cast doubt on the possibility that the radio source is a Cygnus X-1 -like source associated with the γ-ray emission. These results were reported in IAU Circular 5252. Furthermore, a number of successful 10 and 20μm CGS 3 observations were made, marking the first use of this instrument in service time.

Potential users are invited to note that the 2x magnifier is now available for service runs and may be requested for runs in which the 0.6 arcsec per pixel scale is advertised.

Observers and TOs who obtained data for service users included Colin Aspin, Joel Aycock, Mark Casali, Tom Geballe and Dolores Walther. Kevin Krisciunas assisted with data reduction. Thanks to all of them and to our assessors.

John Davies
ROE

CGS 4 in UKIRT VAXnotes

Several topics relating to CGS4 data reduction and observing preparation, including lists of currently known bugs and wish-lists, may be found in the UKIRT VAXnotes conference on the Edinburgh STARLINK node. The moderator of this conference is Phil Puxley (REVAD::PJP).

Phil Puxley
ROE

Remote access to UKIRT INFORM Information

We have recently installed on JAC computers, a MAIL based system that allows anyone with MAIL access to JACH (via DECNet, Internet or, in fact, any other means) to obtain copies of documents in the local UKIRT INFORM system. Users should follow the simple instructions presented below. Any problems and/or comments, (including compliments!) should be addressed to JACH::DOLORES or DOLORES@JACH.HAWAII.EDU.

Users should send an E-mail message to:

UKIRT_INFO@JACH.HAWAII.EDU (Internet)
or JACH::UKIRT_INFO (DECnet)

Commands are sent in the body of the message you send. Several commands may be sent at one time; just put one command per line.

Commands are:

LIST [pattern] Gives brief description of all packages matching "pattern". If pattern is omitted, a description of all packages is sent.

HELP Sends this file.

SENDME package Sends all parts of the specified package.

SENDME package.n Sends part 'n' of the specified package.

Commands may be abbreviated. DIRECTORY is a synonym for LIST.

For each request you make, a transaction log is returned to you indicating the status of the request. The status report will indicate whether the request was successfully completed, and when the file was or will be sent. Large files (> 20 blocks) are sent only during off-peak hours.

The following packages are available:

CALIB	UKIRT standards and calibration sources
GENERAL	General things available at JAC
INSTR	Documentation on UKIRT instruments
REDUC	Data reduction facilities available at UKIRT
SENS	Sensitivities of UKIRT instruments
SOFT	Instrument software on UKIRT
UKIRTSERV	UKIRT service observing information

An example of a request could be a mail message sent as follows:

```
MAIL> send
To:  JACH::UKIRT_INFO
Subject:

LIST
SENDME SENS

CTRL-Z
*exit
```

Mail is then sent to UKIRT_INFO and the documentation requested (a list of what is available and the complete calibration section of INFORM) would be sent to the user via MAIL.

Colin Aspin
JAC

UKIRT Upgrades Update

In the March 1990 UKIRT Newsletter I described the progress which had been made with improvements to the optical performance of UKIRT. After an account of the engineering which had brought the secondary mirror onto the primary axis, eliminating 3rd-order Coma at the zenith, I remarked that we had now done the easy stuff and that what came next would be harder, slower and more expensive. I was right, of course. However, despite the demands on the JAC engineering staff from several directions, notably, the recent advent of CGS4, appreciable progress *has* been made, and so here is another Update.

Current best imaging performance: 0.4 arcsec FWHM!

Recently we acquired the scale-changing fore-optics for IRCAM. During the second set of tests Mark Casali took a series of images of close double stars at a scale of 0.3 arcsec per pixel, to get an idea of the imaging properties of the new system.

He was very pleasantly surprised. In March 1990 I described some of fairly ambitious modifications to UKIRT which, I speculated, could eventually allow UKIRT to "be capable of delivering images with the FWHM of the "telescope" component consistently below 0.5 arcsec". We have not made any of the proposed modifications as yet, but Mark's images already surpass the speculations. Cross sections of an image of the double star B 1837 have FWHM of only 0.47 arcsec *before* correction for the finite pixel size; the intrinsic image size is only ~0.41 arcsec FWHM.

This performance is close to the best achieved by any ground based telescope without the use of interferometry, and is a quite extraordinary endorsement of the competence of Grubb's now-defunct optical workshop (and the conservatism of their specification, which predicted a limiting performance of "only" 0.5 arcsec FWHM) and also of the quality of Mauna Kea seeing.

The catch? There may well be one; the exposures were only 1/6 second. This will have frozen out most of the windshake and may have removed quite a lot of the translation component of the seeing, too. We do not know how often such imaging will be possible: Mark may just have had extreme good luck. However his result has encouraged us to rethink several aspects of the upgrades program, and urgently to pursue the possibility of obtaining a good quality seeing monitor (see below).

Aberrations of the telescope: the primary mirror

Simon Craig has designed a system which uses a 300mm optical flat in place of the secondary and a small TV camera at a pseudo-Newtonian focus. Three series of tests have been carried out in this configuration, in which near- and out-of-focus images and knife-edge images have been obtained.

These have revealed that the primary suffers from variable astigmatism, which is sometimes almost too small to detect in the images, but at other times almost an order of magnitude larger. At any one time this aberration appears to be roughly constant over the sky, and the cause is suspected to be non-reproducible operation of one or more of the mirror support pads. We suspect that if one notices nasty astigmatism, a sensible thing to do might be to switch the telescope off and then on again, re-floating the primary mirror and perhaps unsticking an offending support pad.

Thermal behaviour of the telescope and dome

Early measurements of dome air and structural temperatures were made with a pair of mercury thermometers stuck to appropriate objects with sticky tape. The interesting results inspired the procurement and installation of a more sophisticated system of multi-point temperature measurement which Kent Tsutsui has now brought into initial operation. It measures, in principle, the top and bottom surface temperatures of the primary mirror, the air at four points just above the primary, the air at two points at the top-end, and the top-end steelwork itself. Further sensors are planned, to measure air and structural temperatures halfway up the tube, air just inside the dome apex, and the material temperature of the dome wall.

At the time of writing the system has a number of minor problems: some structural probes are clearly measuring air, and some air probes sometimes touch the structure. Calibration is not yet complete. However some fascinating results have already emerged. The air around the top-end has a typical temperature range of ~13°C, while the top-end structure can have an even larger range: it equilibrates with the air during the day, but during the night it can get appreciably colder than the air, presumably by radiative cooling to space. A need for improved upper dome ventilation is indicated.

The primary mirror varies by only a degree or less through the day, but the air in its vicinity has a range of several degrees. Until the probes are fully calibrated we cannot be certain, but it looks very

much as though the air is nearly always colder, which is bad for seeing: the CFHT measures a dependence of ~0.4 arcsec/(degree$^{6/5}$) of excess temperature of the mirror over the dome air. The biggest temperature differences occur at night.

If it is confirmed that the mirror is in fact degrees warmer than the air *on average* it will be essential to examine the cause of this excess. The obvious suspect will be the ~2kW of heat dissipated by the instrument electronics on the mirror cell. However an experiment at CFHT, which normally has ~10 kW of dissipation in this area suggests that the effect of our heat sources should be much smaller.

Further top-end improvements

By the time this is circulated Simon Craig expects to have installed new, high-performance flexipivots in the secondary mirror support system. These should almost remove the flexure of the secondary assembly as the telescope moves away from the zenith, to the benefit of the pointing, the stability of the thermal background and the optical adjustments.

Further optical tests

An expedition has been planned by Colin Humphries and colleagues from ROE to use an interferometer to characterise the UKIRT optics in more detail and quantitatively. This has been provisionaly scheduled for August 1991. Such tests are essential to make further real progress to understand and improve the UKIRT optical system.

Seeing Monitor

A conceptual design is being prepared for a seeing monitor to enable detailed and quantitative seeing data to be accumulated as a matter of routine. We currently have only a few individual "genuine" seeing measures. With a large suite of such measurements and the results from the temperature measurements we will begin to be able to quantify the dependence of the seeing on the various temperature anomalies in the telescope and dome. Without it, as now, we cannot even specify instruments with confidence that we understand the seeing regimes in which they will mostly be used.

There are other developments, most embryonic as yet. We hope for an upturn in resources, to continue to advance UKIRT still further as the most powerful and versatile IR telescope in the world!

Tim Hawarden
JAC

1990 Refereed Papers from UKIRT Observations

This list is as complete as we can make it. If you know of any omissions or errors, please inform Maureen McLean or Liz Sim; contact information is on the back cover of this Newsletter.

Velocity profiles of high excitation molecular hydrogen lines.
A H Moorhouse, P W J B Brand, T R Geballe, M G Burton 1990 M.N.R.A.S. **242**, 88

Broad infrared line emission from the nuclei of Seyfert 2 galaxies.
P R Blanco, M J Ward, G S Wright
1990 M.N.R.A.S. **242**, 4P

Infrared observations of the eclipsing millisecond pulsar 1957+20.
S A Eales, E E Becklin, B Zuckerman, I S McLean

1990 M.N.R.A.S. **242**, 17P

The molecular hydrogen content of NGC604 and other M33 HII region complexes.
F P Israel, T G Hawarden, T R Geballe, R Wade
1990 M.N.R.A.S **242**, 471

Red giants with unusual dust shells - I The database.
C J Skinner, I Griffin, B Whitmore
1990 M.N.R.A.S. **243**, 78

The alignment of the radio and infrared structures of 3C 356 and its applications for other high-z radio galaxies.
S A Eales, S Rawlings
1990 M.N.R.A.S. **243**, 1P

Controlled bending of a thin mirror to regain figure after warping due to edge cutting.
C M Humphries
1990 M.N.R.A.S **243**, 177

The 3.4 micron interstellar absorption feature in Cyg OB2 #12.
A J Adamson, D C B Whittet, W W Duley
1990 M.N.R.A.S. **243**, 400

The optical and infrared emission of blazars.
K R Ballard, A R G Mead, P W J L Brand, J H Hough
1990 M.N.R.A.S. **243**, 640

Multifrequency variations of the Wolf-Rayet system HD193793 - I: Infrared, x-ray and radio observations.
P M Williams, K A van der Hucht, A M T Pollock, D R Florkowski, H van der Woerd, W M Wamsteker
1990 M.N.R.A.S. **243**, 662

Simultaneous multi-frequency observations of the Seyfert I Galaxy NGC4051: constant optical-infrared emission observed during large-amplitude x-ray variability.
C Done, M J Ward, A C Fabian, H Kunieda, S Tsuruta, A Lawrence, M G Smith, W M Wamsteker
1990 M.N.R.A.S. 243, 713

A combined optical, infrared and radio study of the megamaser galaxy III ZW 35.
J M Chapman, L Staveley-Smith, D J Axon, S W Unger, R J Cohen, A Pedlar, R D Davies
1990 M.N.R.A.S. **244**, 281

A photometric study of BX Andromedae.
S A Bell, P P Rainger, G Hill, R Hilditch
1990 M.N.R.A.S. **244**, 328

Dust around HII regions - II. W49A.
D Ward-Thompson, E I Robson
1990 M.N.R.A.S. **244**, 458

Ice Mantles in Barnard 5 IRS1
S B Charnley, C D B Whittet, D A Williams
1990 M.N.R.A.S **245**, 161

Multi-colour 8-13 μm maps of the central parsec of the Galaxy.
C H Smith, D K Aitken, P F Roche
1990 M.N.R.A.S. **246**, 1

Infrared photometry and spectroscopy of Nova PW Vul 1984
A Evans, C M Callus, P A Whitelock, D Laney
1990 M.N.R.A.S. **246**, 527

Infrared imaging polarimetry and photometry of S106.
C A Aspin, J T Rayner, I S McLean, S S Hayashi
1990 M.N.R.A.S. **246** 565

An optical and near-infrared polarization survey of early - type radio galaxies.
C Brindle, J H Hough, J A Bailey, D J Axon, W B Sparks 1990 M.N.R.A.S. **247**, 327

Globular cluster distances from the RR Lyrae log (period) - infrared magnitude relation.
A J Longmore, R Dixon, I Skillen, R F Jameson, J A Fernley 1990 M.N.R.A.S. **247**, 684

Millimetre and submillimetre molecular line observations of the reflection nebula NGC 2023.
G J White, C Sanderson, T S Monteiro, K J Richardson, S S Hayashi
1990 Astron Ap **227**, 200

Polycyclic Aromatic Hydrocarbons in the near-IR spectra of 24 IRAS sources.
M Jourdain de Muizon, L B d'Hendercourt, T R Geballe
1990 Astron Ap **227**, 526

A search for interstellar dust features in the 3 micron spectrum of NGC 4565.
A J Adamson, D C B Whittet
1990 Astron Ap **231**, 27

SSV13 - a disk-collimated outflow?
G Sandell, C Aspin, W D Duncan, E I Robson, W R F Dent 1990 Astron Ap **232**, 347

Multi-wavelength observations of 3C273 II. 1986-1988
T J Le Courvoisier, E I Robson, A Blecha *et al*
1990 Astron Ap **234**, 73

Optical-infrared photometry of the "isolated" T Tau star V4046 Sgr
M G Hutchinson, A Evans, H Winkler, J Spencer Jones
1990 Astron Ap **234**, 230

IRAS 05341+0852 : an evolved star with unique 3 micron emission features.
T R Geballe, W E C J van der Veen
1990 Astron Ap **235**, L9

Three micron spectroscopy of IRAS sources : observed and laboratory signatures of PAHs.
M Jourdain de Muizon, L B d'Hendercourt, T R Geballe
1990 Astron Ap **235**, 367

Infrared imaging polarimetry of Mon R2 IRS.
C A Aspin, D M Walther
1990 Astron Ap **235**, 387

The 3.4 and 12 micron absorption bands in the proto-planetary nebula CRL 618.
J Lequeux, M Jourdain de Muizon
1990 Astron Ap **240**, L19

Optical and infrared polarimetry and photometry of blazars.

A R G Mead, K R Ballard, P W J L Brand, J H Hough, C Brindle, J A Bailey
1990 Astron Ap Supp **83**, 183

A polarimetric survey of symbiotic stars.
R E Schulte-Ladbeck, C Aspin, A M Magalhaes, H E Schwarz
1990 Astron Ap Supp **86**, 227

The abundance of AsH3 in Jupiter
K S Noll, H P Larson, T R Geballe
1990 Icarus **83**, 494

Elliptical-like profiles in infrared images of merging spiral galaxies
G S Wright, P A James, R D Joseph, I McLean
1990 Nature **344**, 417

Observations of interstellar polarization at 2.2 and 8μm T Nagata
1990 Ap J, **348**, L13

An IR quintuplet near the galactic centre
H Okuda, H Shibai, T Nakagawa, H Matsuhara, Y Kobayashi, N Kaifu, T Nagata, I Gatley, T R Geballe
1990 Ap J, **351**, 89

IR polarimetry of the NGC 6334 V bipolar nebula
T Nakagawa, T Nagata, H Matsuhara, H Okuda, H Shibai, S S Hayashi
1990 Ap J, **351**, 573

Observations of the 4μm fundamental band of $H3^+$ in Jupiter
T Oka, T R Geballe
1990 Ap J, **351**, L53

IR spectroscopy and imaging of the Crab Nebula
J R Graham, G S Wright, A J Longmore
1990 Ap J, **352**, 172

Multifrequency observations of BL Lacertae
J N Bregman *et al.* (26 authors)
1990 Ap J, **352**, 574

A spectacular molecular outflow in the Monoceros OB1 molecular cloud
M Margulis, C J Lada, T Hasegawa, S S Hayashi, M Hayashi, N Kaifu, I Gatley, T P Greene, E T Young
1990 Ap J, **352**, 615

High spectral resolution observations of fluorescent molecular hydrogen in molecular clouds
M G Burton, T R Geballe, P W J L Brand, A Moorhouse 1990 Ap J, **352**, 625

Images of shock-excited molecular hydrogen in young stellar objects
R P Garden, A P G Russell, M G Burton
1990 Ap J, **354**, 232

IR images of ionized and molecular hydrogen emission in S106
S S Hayashi, T Hasegawa, M Tanaka, M Hayashi, C Aspin, I S McLean, P W J L Brand, I Gatley
1990 Ap J, **354**, 242

IR studies of elliptical galaxies II: a radio-selected sample
C D Impey, C G Wynn-Williams, E E Becklin
1990 Ap J, **356**, 62

The exciting star in G35.2N
D M Walther, C Aspin, I S McLean
1990 Ap J, **356**, 544

Discovery of five PMS binaries in Taurus
W P.Chen, M Simon, A J Longmore, R R Howell, J A Benson
1990 Ap J, **357**, 224

Velocity dispersion and the stellar population in the central 1.2 parsecs of the Galaxy
K Sellgren, M T McGinn, E E Becklin, D N B Hall
1990 Ap J **359**, 112

Subarcsecond resolution observations of the central parsec of the Galaxy at 2.2 microns
M Simon, W P Chen, W J Forrest, J D Garnett, A J Longmore, T Gauer, R I Dixon
1990 Ap J **360**, 95

A K band deep galaxy survey
L L Cowie, J P Gardner, S J Lilly, I S McLean
1990 Ap J **360**, L1

Unusual IR line profiles in the post AGB star HD56126
S Kwok, B J Hrivnak, T R Geballe
1990 Ap J **360**, L23

4C41.17: a radio galaxy at a redshift of 3.8
K C Chambers, G K Miley, W J M van Breugel
1990 Ap J **363**, 21

Observations of 5 micron lines of shocked CO and H2 in the Orion Molecular Cloud
T R Geballe, R P Garden
1990 Ap J **365**, 602

A Model of the brightness of moonlight

A knowledge of the brightness of moonlight is needed for detailed calculations of the limiting magnitude of astronomical detectors, whether visual, photographic, or electronic. For example, one might wonder what is the faintest reference star one can see on the UKIRT video screen on a night with a quarter moon 60° from the position of interest in the sky.

Bradley Schaefer (NASA/GSFC) and I have worked out a model and tested it on actual night sky brightness observations.

Let B_{moon} be the contribution to the V-band night sky brightness due to the presence of the moon in the sky. We find that

$$B_{moon} = f(\rho) I^* 10^{-0.4kX(Z_m)} [1 - 10^{-0.4kX(Z)}] \quad (1)$$

Here
Z = zenith angle of sky position measured
Z_m = zenith angle of moon
X(Z) = air mass value of sky position
$X(Z_m)$ = air mass value of moon
k = V-band atmospheric extinction (magnitudes/air mass)
I* = illuminance of the moon outside the Earth's atmosphere.
ρ = angular distance (degrees) between the position on the sky where the sky brightness is measured, and the moon's position in the sky.
f(ρ) = a scattering function, scaled to give B_{moon} in units of nanoLamberts. The scattering function is the same for daytime sunlight scattering or nighttime moonlight scattering, based on observations of each and accounting for the difference of brightness of the Sun and Moon.

Using nanoLamberts for B_{moon} may seem an odd choice. Magnitudes per square arc second are definitely the wrong choice, because magnitudes are a logarithmic scale; in this case B_{moon} would depend on whether one were in a city or not! For the reader who prefers the S_{10}(V) unit - the number of V + 10th magnitude stars per square degree - B(nL) = 0.263 S_{10}(V).

The illuminance of the moon is given by:

$$I^* = 10^{-0.4(3.84+0.026|\alpha|+4\times10^{-9}\alpha^4)} \quad (2)$$

where α is the phase angle of the moon - angular distance in degrees between the Earth and Sun, as viewed from the moon.

The scattering function is composed of two parts, due to Rayleigh scattering and to Mie scattering:

$$f(\rho) = 10^{5.36}[1.06 + \cos^2(\rho)] + 10^{6.15-\rho/40} \quad (3)$$

Lunar sky brightness effect from model[a]

Phase angle (α)	Angular distance between moon and sky position (ρ)				
	5°	30°	60°	90°	120°
30°	5489 (-4.14)	871 (-2.58)	396 (-1.95)	328 (-1.67)	626 (-1.87)
60°	2559 (-3.43)	406 (-1.86)	185 (-1.31)	153 (-1.08)	292 (-1.24)
90°	1028 (-2.42)	163 (-1.13)	74 (-0.72)	61 (-0.57)	117 (-0.67)
120°	297 (-1.33)	47 (-0.46)	21 (-0.26)	18 (-0.20)	34 (-0.24)

[a]values of B_{moon}, measured in nanoLamberts. For lunar zenith angle of 60° and V-band extinction of 0.113 mag/airmass (median extinction at Mauna Kea summit). For this table ρ is measured along the great circle passing through the Moon and the zenith. Therefore, the column ρ = 60° corresponds to the zenith. Values in parentheses are ΔV in mag/sec^2, using V = 21.587 mag/sec^2 (B_{zen} = 79.0 nL) as the nominal zenith sky brightness, and scaling the zenith sky brightness to the nominal value at the zenith angle corresponding to ρ.

Finally, we need to calculate the air mass values. A formula based on Eq. 29 of Garstang gives the best fit for sky brightness measures, whether the moon is on the horizon or high in the sky:

$$X(Z) = (1 - 0.96 \sin^2 Z)^{-0.5} \quad (4)$$

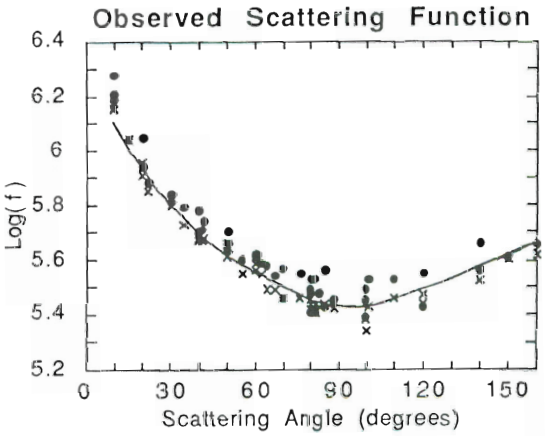

Figure 1. The scattering function f(ρ) as deduced from observations of the daytime sky at two sites in the Soviet Union. The function given in Equation 3 is plotted as a smooth curve.

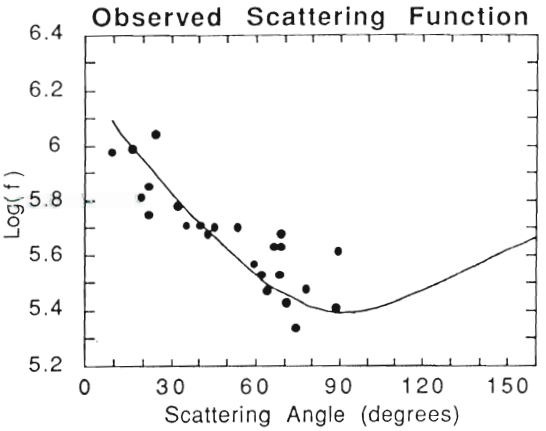

Figure 2. The scattering function f(ρ) as deduced from moonlight observations made by Krisciunas at the 2800-m level of Mauna Kea. The function given in Equation 3 is plotted as asmooth curve. The greater scatter of this diagram, comparedto Figure 1, derives from uncertainties in the raw observations and in subtracting out the contribution of the non-zero sky background that is present even when there is no moonlight.

Let the zenith V-band sky brightness *without moonlight* be V_{zen}, in magnitudes.arcsec^{-2}. The sky brightness in nanoLamberts will be:

$$B_{zen} = 34.08 \exp(20.7233 - 0.92104\, V_{zen}) \quad (5)$$

The dark nighttime sky brightness (B_o) increases due to airglow as a function of zenith distance (Z) and is given by:

$$B_o(Z) = B_{zen}\, 10^{-0.4k(x-1)}\, X \quad (6)$$

Finally, the change in the V-band sky brightness, measured in mag.arcsec^{-2}, due to moonlight will be

$$\Delta V = -2.5 \log[(B_{moon} + B_o(Z))/B_o(Z)] \quad (7)$$

We find, from a comparison of the model to a data set of 33 observations made at the 2800-m level of Mauna Kea from September 1985 through January 1991, that the model fits the data with an RMS error of about 23 percent. Measurements of scattered sunlight give an RMS error of only 8 percent. The larger error for the moonlight data (model vs. observed) results from uncertainties in the contribution of faint stars in the beam and uncertainties in the extinction corrections.

As a guide, we have tabulated typical values of B_{moon} (in nL) and ΔV (in magnitudes.degree^{-2}) for a range of α and ρ. The table was constructed with the assumption that k = 0.113 mag/airmass (median V-band extinction at the Mauna Kea summit), and that V_{zen} = 21.587 mag/sec^2 (mean dark sky value measured at the 2800-m level of Mauna Kea, equivalent to B_{zen} = 79.0 nL).

For sites with V-band atmospheric extinction greater than the Mauna Kea summit value, the moonlight contribution to the sky brightness is greater than the tabulated values because the moonlight contribution comes from scattering of light, and where one observes through more atmosphere (i.e. closer to sea level), there will be more scattering. At the other end of the scale, where the extinction k = 0 (i.e. in Earth orbit), B_{moon} = 0 (i.e. the sky is black even with the Moon or Sun visible).

Kevin Krisciunas
Joint Astronomy Centre

References

Krisciunas, K & Schaeffer, B. PASP (in press)
Garstang, PASP **101**, p.306, 1989

JCMT Instrumentation and Observational Sensitivities for Semester V.

The instrumentation which should be available to JCMT users semester V (February - July 1992) is summarized. Further details can be found in 'The James Clerk Maxwell Telescope: A Guide for the Prospective User', which is available from JCMT Section at ROE, the JCMT Group at the Herzberg Institute of Astrophysics in Canada, or from me.

Spectral Line Observations

Receivers A1, A2

Receiver **A1** is a dual-channel Schottky device for heterodyne observations covering the frequency range 216 to 280 GHz. On the telescope, typical double-sideband receiver temperatures for A1 at the band centres are 350 K and 650 K for the lower and upper bands respectively, corresponding to single sideband system temperatures of ~900 and 1500 K respectively in the best cases. Receiver temperatures increase with distance from the band centres. A single-sideband filter should be available for rejection of the image sideband; it should be specifically requested in the proposal.

The SIS receiver **A2** is expected to be commissioned during semester V and may be made available to users on a best efforts basis. However, no specific requests for its use in semester V can be entertained, and no firm performance values can be given yet. It should cover the same frequency range as A1, with a SSB system temperature of 400K.

Receivers B2 and B3(i).

B2 is a dual-channel Schottky mixer system for spectral line observations in the range 330 to 360 GHz. The system temperatures obtainable on the sky under good conditions are between 1500 and 2000K throughout this band.

B3(i) is an single-channel SIS receiver which will be commissioned in semester U. It should cover the frequency range of ~310 to 380 GHz, with SSB receiver temperature projected to better than 300K throughout the band, corresponding to a system temperature of about 900K under good conditions.

Since the availability of B3(i) is uncertain in semester V, proposals for the frequency range 330 - 360 GHz should base time estimates on the performance figures for B2. Proposals requiring frequencies below 330 GHz or above 360 GHz may be accepted on a 'shared risks' basis, depending on progress on B3(i) in the interim, and scheduled contingent on the status of the receiver at the time.

Table I

Frequency (GHz)	Receiver	T(rx) (K)	T(sys) (K)	dv (MHz)	Rms noise (K)	η_{fss}	η_l	Notes
230	A1	350	960	0.33	0.08 (0.07,0.11)	0.77	0.91	
270	A1	650	1600	0.33	0.13 (0.11,0.18)	0.77	0.91	
330	B2	680	2140	0.33	0.18 (0.16,0.67)			
345	B2	560	1720	0.33	0.14 (0.12,0.32)	0.70	0.89	
461	C1	560	30800	4.00	0.72 (0.41, *)	0.73?		1,2,3
492	C1	900	76000	4.00	1.79 (1.25, *)			1,2,3
690	G	3000	48300	1.00	2.28 (0.97, *)			2,3
810	G	4000	78800	1.00	3.71 (1.43, *)			2,3

Notes:
(1) This assumes a total of 50 channels in the spectrum and dual-channel operation.
(2) An '*' means that observations are not possible when conditions are 'poor'; the rms noise is effectively infinite.
(3) Awaiting reports or further commissioning for η_{fss}, η_l, where η_{fss} is the efficiency for forward spillover and scattering

Receivers C1 and C2(i).

Receiver **C1** is a dual-channel 'hot electron' bolometer system designed for observations of CO J=4→3 (461.04 GHz) and neutral carbon $^3P_1$-$^3P_0$ (492.16 GHz) lines. For the form of mixing used, the practical single-sideband IF bandwidth is a little less than 2 MHz and the local oscillator frequency must be 'swept' across the line to obtain a spectrum.

Typical receiver temperatures are better than 800K at 461 GHz, and ~1300 K at 492 GHz for each mixer, or ~550 and 900K if both mixers are used at the same frequency. Under reasonable sky conditions, this leads to total system temperatures of ~3000 and 7000 K per channel, or 30,000 and 70,000K respectively for a 50-channel spectrum.

C2(i) is a single-channel SIS receiver to cover frequencies from 450 to 500 GHz. It is likely to be commissioned in semester V. Proposals cannot yet be accepted for C2(i), but if it were available at the time of observations, proposals for C1 could use it.

Receiver 'G'

This is a dual-channel Schottky device employing a laser local oscillator arrangement. Consequently, only certain discrete frequencies can be accessed, in particular in the regions around the CO J=6→5 and 7→6 lines at ~690 and 800 GHz respectively. Typical double sideband receiver temperatures are from 3000 to 4500 K; specifically, at CO(6→5) and ^{13}CO(6→5) receiver temperatures of 3000 and 3500 K are obtained. The resulting single-sideband system temperatures are extremely sensitive to atmospheric conditions, but are likely to be about 55,000K or more under practical conditions.

Receiver 'G' is on loan from the MPE group in Garching and observers interested in using it should contact either Prof. R. Genzel or Dr. A. Harris to arrange collaborative efforts.

Spectrometer Backends

Two spectrometer systems should be in use.

The new **Digital Autocorrelation Spectrometer (DAS)** is scheduled to be commissioned in January 1992, and may be offered to users during semester V. The DAS has 2048 delay channels having a total maximum bandwidth of 2 GHz. It will be capable of a wide range of configurations, with spectral resolutions of between 0.1 and 1.0 MHz.

The **AOSC** is an acousto-optical spectrometer offering a resolution of about 330 kHz and a total bandwidth of 500 MHz for a single IF channel.

Approximate rms sensitivities after 30 minutes' integration

Table I gives the calculated rms noise in Kelvin after a total observation time of 30 minutes (15 minutes on source, 15 minutes on a reference position) for three different values of atmospheric

Table II

Filter Wavelength (mm)	(micron)	Centre frequency (GHz)	Bandwidth (GHz)	Aperture (mm)	Beamwidth (arcsec)	NEFD (65mm ap) Jy√(sec)	Notes
2.0	2000	150	40	65	28	2.0 (2.0,3.0)	1
1.3	1300	333	64	65	21	0.3 (0.3,0.5)	
1.1	1100	264	75	65	19	0.3 (0.3,0.7)	
0.85	850	354	30	47	16	0.8 (0.7,5.0)	
0.8	761	394	103	47	14	0.7 (0.5,5.0)	
0.75	730	411	28	47	14	not available	2
0.6	625	480	119	36	9	not available	3
0.45	438	685	84	27	7	6.0 (4.0, *)	4
0.35	345	870	249	21	6	12. (8.0, *)	4

Notes:
(1) At this wavelength the UKT14 optics is poorly coupled to the JCMT.
(2) Not yet commissioned. Values will be somewhat greater than for the 0.85μm filter.
(3) This filter is best avoided. It is difficult to obtain consistent calibrations, due to deep atmospheric absorption lines in the window.
(4) Observations are not possible under 'poor' conditions at these wavelengths.

transmission. Expected values of the rms noise are given in parentheses for 'exceptional' and 'poor' conditions (about 0.5 and 5 mm of water vapour respectively). Atmospheric conditions affect receiver B, C and G observations strongly, and in poor conditions work at the higher frequencies becomes impossible.

Continuum Observations

UKT14

The UKT14 bolometer system will be available during Semester V with filters for observations at 2, 1.3, 1.1, 0.85, 0.8, 0.75, 0.6, 0.45 and 0.35 μm. The aperture of the bolometer can be adjusted between 21 and 65 mm. Sensitivities range from typically 0.3 Jy/√(Hz) through to 10 Jy/√(Hz) or more under good photometric conditions.

The properties of UKT14 using the available filters and apertures are given in Table II. The value of the NEFD given is that which should be obtained under 'good' conditions for a 65mm aperture; users should use this value to estimate time requirements. In parentheses, values for the 'best' and 'poor' atmospheric conditions are given to indicate typical ranges obtained.

UKT14 polarimeter

The Aberdeen/QMW polarimeter will be available during semester V as an optional accessory for the UKT14 bolometer system in step and integrate mode. The effective NEFD of the polarimeter-plus -UKT14 combination is NEFD(p) = 2xNEFD/P, where P is the degree of polarization of the source.

Henry Matthews
JAC
June 1991

From the July PATT meeting

At the July PATT meeting, observing time on JCMT was awarded to 47 of the 93 new proposals and the one long-term proposal considered. The oversubscription rate, in terms of the ratio of time applied for to time available, was 2.5. One night was awarded to the Canadian Service Observing Programme - e-mail contact PAF@NRCVM01.

News from the Board Meeting

The ninth meeting of the Board was held in Hilo on May 6-8. In addition to the business sessions, there were astronomical and technical presentations from JCMT observers and staff members. This was the last meeting chaired by Sir Robert Wilson; it was announced that Dr Don Morton will be the next Chairman.

Director, JCMT

The JCMT Board supported the creation of a new post of Director, JCMT, who would be responsible for the whole JCMT project, both operations and development. It is intended to advertise the position and make an appointment as soon as possible. Meanwhile, the Director ROE has appointed Richard Wade to be the Acting Director, JCMT.

Sub-millimetre array telescope for Mauna Kea

Professor Hall announced that the Smithsonian Institute had approved a proposal to locate a 6-dish sub-millimetre array telescope on Mauna Kea. A site to the north of JCMT has been identified and was expected that operation of the telescope would begin in 1994/5.

JCMT Receiver construction programme

The Board endorsed the recommendation of the Receiver Working Group that a Head of the JCMT Receiver Programme be appointed. They agreed that this person should be guided by other recommendations of the Working Group, such as the establishment of a small management team, the more extensive use of external project scientists and the targeting of receiver construction contracts.

SOLAR ECLIPSE of JULY 11

The eclipse was successfully observed with the JCMT working at a wavelength of 1.2mm. The international consortium which had been awarded telescope time completed their programmes on the chromosphere and corona; we hope to include a full report in the next Newsletter.

Remote Observing with JCMT

Remote observing is now available with the JCMT, from any suitable site in the UK, Canada and The Netherlands. All JCMT instruments should be usable. The remote observing system is similar to the one that has been developed on UKIRT, and it is very easy to use. A remote observer (RO) logs on to one of the remote-observing usernames at the JCMT and selects from a menu which observing screens (s)he wants to see. Usually the RO has a separate login for each screen, although it is also possible to swap between screens from a single login. There are mechanisms for file transfers and for communications with people at the telescope.

Although active remote observing is possible with this system, only passive observing will be permitted at present. With passive observing the RO watches progress at the telescope but does not control any of the observations. With active remote observing the RO would also be able to control the observations.

A draft manual exists that describes, mainly, the facilities for remote observing with UKIRT; it is presently being expanded to incorporate the more recent remote observing with the JCMT. Copies of the current draft are available on request.

Any site which can be connected through Internet should be usable for remote observing. ROs in the UK will be able to use the 56 kbit/sec dedicated line from the UK to Hawaii, which is available from Starlink and Janet nodes. This line has generally been working well, with only a few occasional breakdowns. Compressed voice channels from ROE will also operate across the line following the delivery of some hardware, which is presently scheduled for mid-July.

Observers are encouraged to participate in remote observing with the JCMT. At this stage however it is still expected that one member of the observing team will travel to Hawaii.

Potential remote observers should contact me for further details. They should also contact their assigned support scientist for discussions about feasibility and for authorisation.

Roger Clowes

Starlink: REVAD::RGC
Janet: RGC @ UK.AC.ROE.STARLINK
SPAN: 19527::REVAD::RGC
Internet: RGC @ STARLINK.ROE.AC.UK

JCMT Bulletin Board - VAX Notes Conference

I have set up a JCMT Bulletin Board as a VAX Notes Conference on the VAX cluster at the ROE. This is provided as an information exchange for all users or potential users of the JCMT to help us get the most out of our use of the telescope. If you have access to a VAX running VAX Notes (eg. on Starlink) you can participate directly. You can add the conference to your NOTEBOOK by

ADD ENTRY REVAD::JCMT on Starlink,
or
ADD ENTRY 19457::REVAD::JCMT
from SPAN.

Besides reading entries, you can contribute to the discussion on an existing topic using REPLY or initiate a new topic using WRITE.

Peredur Williams
ROE

The Captive Account JCMTINFORM

There is now a captive account JCMTINFORM which contains information on the JCMT, its use and related matters. To extract the information you want you have to (remotely) login on the VAX at ROE (UK STARLINK users: set host revad). The username is JCMTINFORM and you are then entering a menu driven, self-explanatory program. For UKIRT users there will be a "déjà vu" experience, indeed it is build up in the same way as UKIRTINFORM. You can either read the information on your terminal or copy the files you need into your own area, print them and read them at leisure.

Some information is very extensive or in the form of figures and for these topics printouts are available from the JCMT Unit at the ROE. This applies in particular to the "basic" pieces of information that every (first time) user should read:

1) Introductory Information for Visitors to Joint Astronomy Centre
2) The James Clerk Maxwell Telescope: A Guide for the Prospective User

For complaints, updates, printouts and questions about JCMTINFORM please email Ko Hummel (kxh@UK.AC.ROE.STARLINK)

Ko Hummel
ROE

Estimating required integration times and limiting sensitivities for the Aberdeen/QMW Polarimeter

The only method of doing polarimetry with the above polarimeter plus UKT14 that has been successfully proven to date is simply to carry out normal photometry at different waveplate positions and to estimate the polarisation parameters from the resulting modulations (so called *step and integrate* mode). For a single step and integrate cycle the signal to noise ratio in the determination of the degree of linear polarisation is approximately given by:

$$\left(\frac{S}{N}\right)_{pol} \sim \frac{T_{pol}\sqrt{nt}\; pF\eta_{pol}}{\sqrt{2}\,(NEFD)} \qquad (1)$$

where n is the number of waveplate positions used, t is the integration time at each waveplate position, *NEFD* is the noise equivalent flux density of UKT14, F is the source flux density, p is the source degree of linear polarisation, T_{pol} is the overall transmission of the polarimeter (waveplate plus wire grid polariser) for unpolarised radiation $T_{pol} \sim 0.47$ for all three waveplates i.e. 450μm, 800μm and 1100μm) and η_{pol} is the polarisation modulation efficiency of the polarimeter ($\eta_{pol} \sim 0.95$ for all three waveplates).

Note that if we have a polarisation detection we can average N such cycles and achieve a $\sqrt{N}$ improvement in the above signal to noise ratio.

The accuracy of the determination of the polarisation position angle, θ, associated with p can be estimated from the 'standard expression' (Serkowski):

$$\Delta\theta \sim \left(\frac{S}{N}\right)_{pol} \times 28.6^{\circ} \qquad (2)$$

As an example, for the typical step and integrate cycle of 10 waveplate positions with 20 seconds integration at each position, as used during the polarimeter commissioning (Flett and Murray), we get the following approximate expression for the minimum detectable polarised flux ($(S/N)_{pol}=1$):

$$(pF)_{\min} \sim \frac{NEFD}{4.5} \qquad (3)$$

This yields values of pF_{min} at 1100μm and 800μm (for UKT14 *NEFD*'s of 0.3Jy/√Hz and 0.7Jy/√Hz) of 67*mJy* and 156*mJy* respectively. These figures agree favourably with the empirically found minimum detectable polarised fluxes of ~100-200*mJy* at 800μm and 1100μm achieved during the commissioning runs under 'average' sky conditions.

A few final points should be noted:

1. The cycle time is a compromise between spending long enough at each point to get reasonable photomtery and completing one cycle (and hence obtaining one estimate of the polarisation parameters) in sufficiently short a time that drifts in sky transparency/emmission and changes in polarisation parameters due to sky and tertiary mirror rotations do not 'wipe out' the required modulations.

2. This analysis assumes that the instrumental polarisation is something that is accurately known and can be subtracted off without introducing further error. In reality this subtraction will degrade the above signal to noise ratios and probably limit measurable polarisations to ≥ 0.2%

3. The analysis does not allow for time spent in calibrating and characterising the instrumental polarisation or in moving the waveplate and telescope or for the settling time after such motions. Together with the usual pointing and focussing checks this may consume up to 50% of the telescope time.

4. The problems and limitations introduced by the atmosphere are if anything more severe for polarimetry than for photometry with UKT14.

Sye Murray
Queen Mary & Westfield College,
London University

References

Serkowski, K. 1974, *Methods of Experimental Physics*, **12.**, Part A, ed. N. Carleton (New York: Academic press).
Flett, A. M. and Murray, A. G. 1991, M.N.R.A.S., **249**, Short Communicatons, 4p-6p.

DBMEM - Dual beam mapping with a maximum entropy algorithm

Continuum mapping observations at the JCMT using the UKT14 bolometer are almost always done in 'on-the-fly' mode, where the telescope scans continuously in azimuth whilst simultaneously chopping the beam in azimuth with the secondary mirror; RxA or RxC is used as the backend. The chop throw at the JCMT is limited by atmospheric effects and beam distortion to ~40 arcsec at the higher frequencies, and because many sources are bigger than this, the source structure is confused by the chopping. In addition, throughout the map the source's parallactic angle changes so that the data points lie on a non-regular grid in the RA-Dec frame. These two problems make it necessary to use image reconstruction techniques of some sort to make pictures from the on-the-fly maps.

Most continuum observers currently use the Emerson-Klein-Haslam (EKH) algorithm (A&A 76, 92), a two step algorithm implemented as the RESTOR and CONVERT programs in the NOD2 library. After pre-processing the data (de-spiking and base level subtraction), the effect of chopping is removed by a Fourier filter (program RESTOR), and the final map in RA-Dec coordinates is made by interpolation of the azimuth-elevation map.

In May 1990 I obtained some JCMT on-the-fly maps of the bipolar nebula S106. In the process of reducing them I became interested in the mapping algorithm. There were two problems I felt NOD2 was unable to deal with effectively. First, how to combine several on-the-fly maps to make a single final map; coaddition of maps in NOD2 seemed to give smooth maps of lower resolution than should be attainable with the JCMT. Second, in my 450 μm map I knew that at least half the detected power on an extended source was picked up through the error pattern and I wanted a way of taking account of this by doing a true beam deconvolution.

Making sky images from dual beam data is in fact a deconvolution problem (*cf* HST) but with a twist: the point spread function varies across the map. Whilst not leading to severe conceptual problems it does lead to computational ones. I have implemented a solution to this linear inversion problem using a maximum entropy method using the MEMSYS3 subroutine library of Gull and Skilling, and have tested its performance using both synthetic and real data sets (two related papers have been submitted to MN - on observations of S106, and the algorithm itself). Initial results from the program (DBMEM) are very encouraging and certainly an improvement on the traditional NOD2 processing. The main caveat is the larger processing time required and significant memory requirements; at present 'quick-look' data reduction by this method at the telescope is impossible.

The figures show two comparisons of the EKH and DBMEM methods. Figure (1b) is a model sky brightness distribution. A dual beam observation of this source (with a 14 arcsec beam) was simulated and restored using the two methods. The DBMEM image (1c) is clearly superior to the EKH image (1a). Figure 2 shows the two methods applied to real data (an 1100μm JCMT map of S106); again the presence of the higher spatial frequencies in the DBMEM map is apparent.

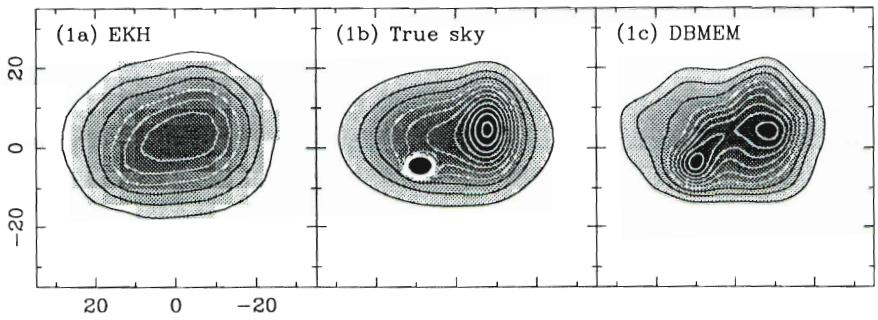

I hope soon (October) to make the programs available to the community as I believe they represent a significant improvement in image quality. Users should be aware that the MEMSYS3 code is made available to STARLINK by Gull & Skilling on the understanding that all users sign a license agreement prior to using the code.

John Richer
Mullard Radio Astronomy Observatory, Cambridge.

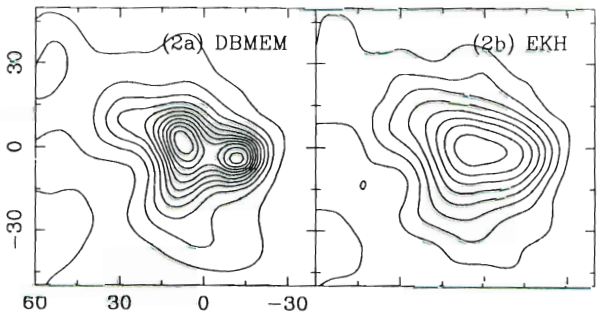

The JCMT Support Scientist Corner

In the last issue I discussed techniques for mapping with UKT14, our continuum bolometer. This time I will briefly discuss how to calibrate maps, because I have a feeling that there is a lot of uncertainty in how this should be done. Neither have we ever had time to provide any decent recommendations of how it should be done.

The key to calibrating maps is to obtain accurate photometry. The photometry enables us to keep track of extinction, which is normally the biggest source of uncertainty, especially at short wavelengths, but by no means the only one. Other ways of keeping track of the extinction are by doing skydips, using the UKT14 calibration unit, and using information from the CSO 1.3mm sky monitor. However, knowing the extinction is not sufficient. We also need to know the beam shape accurately, not only the half power beam width (HPBW), and also the error lobe contribution. This is a non trivial task, because it is time consuming, and most observers therefore prefer to believe that these quantities are well known. This is not the case. The JCMT dish is adjusted so frequently that even active observers like myself have severe difficulties in keeping up with all the changes. During the last year I have obtained quite a few beam maps of the diffraction-limited 450μm beam. From these maps (all taken with chop throws of 20 or 30") I find HPBWs ranging from 7.4" to 8.6" in good weather conditions. Why the spread is so large I don't fully understand, but note that a 1" error in the HPBW translates to a calibration uncertainty of 25 - 30%. What is also important to note is that the error lobe pickup is non negligible at all UKT14 wavelengths.

Why is this the case? First of all, most of the mapping is done at short wavelengths, i.e. 800 or 450 μm, where the surface errors clearly start to show up, even though the surface accuracy of JCMT is amazingly good for a 15m telescope. But even at 1.3mm I have reasons to believe that the error lobe contribution cannot be overlooked. This is due to the way UKT14 illuminates the surface. UKT14 has at most a 3dB taper, which gives us a nice narrow main lobe, but large sidelobe contributions. At 1.3 and 2mm, the illumination is even more uniform, resulting in large sidelobes. Just to give an idea of what the amount of the error lobe pickup is, I find that mapping over a 60" x 60" area we have an error lobe contribution of 22 - 25% at 800μm, 30 - 60% at 450μm, and 100% or more at 350μm. Note that I quote rather large uncertainties for the 450 and 350μm error lobe contributions. This is simply because at these wavelengths there are so many parameters affecting the error lobe. It depends on how well the telescope is focused; the HPBW and the associated error lobes are almost certainly elevation dependent, and they are definitely a strong function of chop throw. In addition our measurement accuracy may be affected by refraction noise, which is quite often present, especially in early evenings and late mornings.

After these few words of caution, let me now give you a quick guide through continuum map calibration:

1. We have determined the extinction, either using photometry of planets and/or secondary calibrators, and perhaps using skydips as well. From these data we also determine the flux conversion factor C, which is a function of filter, aperture, and chop throw. The most accurate determination of C is obtained from a calibrated beam map of a planet (see below). Anyway, the assumption is now that we know the zenith opacity before and after the map, as well as the conversion factor between Jy and mV, the instrumental units for UKT14.

Most of the time we map using diffraction limited beams and using very small chop throws, and we may not have a point source from which we can determine the flux conversion factor. It is also very difficult to perform accurate photometry with a narrow Gaussian beam, because the beam is very sharply peaked, and the photometry will be largely dominated by pointing and tracking errors. We therefore normally determine the flux conversion factor directly from a beam map of a planet, i.e. we follow the procedure outlined below, except that we now omit the flux conversion factor, the quantity we want to determine. The end result is therefore a map of the beam in mV, corrected for extinction. The peak signal in the map, V*max (determined from the maximum signal or a Gaussian fit), should therefore correspond to the flux of the planet, corrected for beam coupling (Sbeam), hence C = Sbeam/V*max

2. If we have done a NOSWITCH map, i.e. no nodding between the positive and the negative beam , we first need to scale the map by a factor of two, to bring it in accordance with our photometry scale, which is the difference between the signal and reference beam, i.e. twice the signal level in a map. If we have done the map in on-the-

fly mode, we also need to account for the scaling which occurs when we feed the signal into the RXA or IFD micro (the latter is preferred). This scaling factor is sensitivity/10 for RXA and sensitivity/5 for IFD. Note that the sensitivity is set by the observer in the UKT14 software, it is a quantity which is not stored in the data files (because of the ad hoc arrangement of on-the-fly mapping and its incompatibility with the rest of the JCMT software), and it therefore has to be written down. Please don't forget it. After these two scaling factors have been applied, we now have the data back to the same mV scale as used by UKT14, the rest is therefore easy. We take the base level and deglitched (spike corrected) map and multiply it by these two factors. In the case of a grid map (never done anymore, because of the large software overheads) one would just omit the second scale factor, which is only needed if the data are fed through the IFD and RXA micro. I.e. we multiply the basic map by

K1 = 2 * sensitivity/5 IFD - backend

or 2 * sensitivity/10 RXA - backend

3. To get the map into our final calibration scale, Jy/beam, we just have to scale the data by the flux conversion factor C, and the zenith optical depth. The extinction correction should be applied before the map is restored (in case of a dual beam map), because we apply a sec(z) correction for each point in the map. If the extinction has varied throughout the duration of the map, there is not much we can do, except to assume that the extinction has increased or decreased linearly as a function of time. If we have additional information, like a sudden change in humidity or a clear change in the 1.3mm optical depth from CSO we can try to apply a piece wise linear function of zenith opacity, but it will not be accurate. The CSO opacity is measured in one direction only, and if we look at another portion of the sky, we will almost certainly have a time lag in the change of the opacity. Anyway, assuming that we have coped with the extinction correction, we have now obtained a basic calibrated map.

4. If our map shows compact sources as well as extended emission, we naturally want to know what these fluxes are. To a first approximation we can determine the flux of a point source by doing a Gaussian fit to the final map. To obtain a measure of the extended emission we have to integrate over the map. In this case we have to correct done a beam map of a planet the same night, we can integrate over the same area in the beam map to determine the error lobe contribution. Let's say that we have done a diffraction limited map at 450μm as well as a beam map of Mars. From the calibrated 450μm beam map we have determined a HPBW of 8" and an error lobe contribution of 45% in a 60" x 60" area (by integrating over the map and finding the ratio (integrated flux)/(total flux of Mars) = 1.45). In this case we would therefore divide the integrated flux in the map by a factor = 1.45, if we have determined the integration over the same area in our map. Omitting the error lobe contribution at 450 and 350μm will therefore result in large errors.

Ideally one would like to remove the error beam from the data, either by maximum entropy or some cleaning algorithm, but this requires beam maps of high signal to noise, which are generally not available. For the moment an even more severe restriction is lack of suitable software, but I am sure that this restriction can be overcome.

Göran Sandell
JAC

SPECX Notes.

Documentation.

SPECX V6.1 has now been distributed to Starlink sites. It continues the war against bugs, and includes a few new features (extra functions etc) that were not in V6.0A, which many of you by now may have used at the telescope. An up-to-date LaTeX manual is distributed with the program, so if your site doesn't have a convenient hardcopy lying around, you can print one out for yourself. The LaTeX source files and auxiliary files (.AUX etc), as well as the postscript for the figures, are distributed in the [SPECX.DOC] subdirectory. Just find out where SYS_SPECX points on your system, and then set default to that[.DOC] and you should find it all.

Note that the manual uses encapsulated postscript figures, so it is best to print it on a postscript printer of some sort. Most programs for printing DVI files (I use PSPRINT) will then pick up the references to postscript figures and include them at the appropriate point in the text. If on the other hand you need to edit out the references to the "\special" command, you will need to re-LaTeX the file and redo the index to get the page references

right. It might be better just to comment out the "\special" commmands, and to leave the figures blank...

Import and Export of other formats.

Although FITS format is in some sense now "standard" there are many radioastronomical observatories that do not yet provide FITS output. One problem is that most of us are waiting for the new "final" definitions of single-dish fits, and don't really want to invest a lot of work in a format which may never catch on. In the meantime, lots of people have invented their own format conversion programs. Their efforts have been distributed with SPECX V6.1 in the [.IMPORT] directory tree. At present this includes:

[.IMPORT.FCRAO] - reader for data from Five Colleges Radio Astronomy Observatory (Joan Lasenby, MRAO). Note that this contains two programs; one (FCCOPY) to read the MODCOMP tape, and the second (READIN) to translate the resulting disk file to SPECX native format.

[.IMPORT.ONSALA] - reader for Onsala Space Observatory data (Mike Cox, MRAO). Very similar to the FCRAO reader - programs are ONCOPY and READIN.

[.IMPORT.NRAO8BEAM] - reader for data from the NRAO 8-beam array receiver (Ned Ladd, CfA). The program is NFLPDFL.EXE

[.IMPORT.UMASS_SURVEY] - a reader for the University of Massachusetts CO 1-0 survey data, which is distributed in FITS format (Paul Scott, MRAO). This has not been used for some time and may need some maintenance.

[.IMPORT.IRAM] - This reads standard binary FITS spectra from IRAM and SEST (John Richer, MRAO). This is based on the Starlink TAPEIO and FITS routines written originally (I think) by Jon Fairclough. The format is described in the CLASS manual. (program IRAM_FITS_TO_SPECX).

[.IMPORT.RXG] - This reads the data files produced by the RxG AOS *directly* into SPECX, using an external subroutine (John Richer MRAO, and Adrian Russell, MPE). (The source is in EXTRNL4.FOR).

As well, data from the Nobeyama 45-m is now supplied in FITS (with tables extension), and I believe that Brian Heaton and Malcolm Currie at RAL have now solved the problem of reading that into SPECX via NDF files.

The authors of these programs have kindly consented to their distribution in this form, but note that these are intended mainly as a *guide*; if you have data from another telescope one or other of the above programs will probably give a pretty good indication of what you need to do to be able to read it. Formats change, and there is no guarantee that a program that has worked in the past will continue to work in future.

For export there are the rudimentary SPECX commands, WRITE-ASCII-SPECTRUM and WRITE-ASCII-MAP, whilst a binary mapfile suitable for mapping to an array in a FORTRAN program is generated as mapplane.tmp each time SPECX makes a map of some sort - just rename this file to prevent it being deleted when a new map is produced. I hope to release a proper FITS writer with the next version (always assuming that the dust has settled by then and we know what the FITS format will actually look like).

More interestingly, many sites run both SPECX and GILDAS. Each have their strengths and weaknesses, so as well as John Richer's IRAM FITS reader (see above), the current version of SPECX has a new command WRITE-GILDAS-IMAGE which allows you to dump the current map-cube directly into a GILDAS image cube. You still have to use the GILDAS "HEADER" command to correct most of the header information, and worse, GILDAS actually expects the cube to be ordered with the declination or Y axis running the other way (and can't turn this around to plot it the right way up, although it does label it correctly), but with luck these deficiencies will be remedied with the next release of SPECX.

Happy format converting!

Rachael Padman
MRAO

New results

CGS4 Observations of the redshift z=2 quasar 1331+170

Early in the commissioning of CGS4 a low resolution spectrum was obtained of the redshift z=2.09 quasar 1331+170 covering the 1.6μm window. The aim was to see how well CGS4 performed for faint stellar objects, and, scientifically, to measure the strengths, redshifts and profiles of the redshifted optical forbidden [OIII] 0.4959 and 0.5007 μm lines in a high redshift quasar for the first time. A good signal-to-noise spectrum was obtained in the remarkably short on-target exposure time of 24 mins. The spectrum shows clearly a broad redshifted Hβ line, and longer wavelength narrower features arising from the [OIII] lines in the usual 1:3 flux ratio.

1331+170 was chosen because optical spectra have shown that there are large velocity differences between the low ionization lines from species such as MgII & OI, and the high ionization lines from CIV and CIII (and, anomalously perhaps, Lyα) amounting to about 1500 km/s. Where such velocity shifts are seen, it is almost invariably true that the high ionization lines are blueshifted with respect to the low ionization lines. 2μm spectra show that Hα generally behaves like the low ionization lines, and does not agree well with Lyα. Explanations of these velocity differences require that at least one of the ionization components is flowing into, or out of, the quasar, and is suffering some form of obscuration so that we are not seeing the true projected velocity field. The question is, which component?

The measurements of the forbidden [OIII] lines help us to answer this question. Since these lines arise in low density regions further from the quasar energy source, and are quite narrow, they provide good estimates of the systemic redshift for the quasar. In 1331+170 the [OIII] redshift and the low ionization line redshifts agree well, so we are led to the conclusion that the high ionization material is suffering systematic motion and obscuration in this object. Also the Hβ redshift agrees well with that from [OIII], further reinforcing the finding that the Balmer lines are at the same redshift as the low ionization lines.

Of course, a single observation does not answer all the questions. We do not know if the high ionization material is flowing out from the quasar and obscured by an accretion disk, or if the material is flowing in and suffering internal obscuration. Nor do we know why the Balmer lines and Lyα appear to come from different regions - either dust absorption of Lyα or collisional effects in the low ionization line regions affecting the Balmer line fluxes could account for this, but we do not know which effect is dominant. These are questions which detailed line profile and variability studies may resolve in the future.

These initial observations have shown how sensitive a system CGS4 has proven to be, allowing observations of faint objects with quite short integration times. Of course, the observations of 1331+170 provide only one example of what this remarkably versatile spectrograph is capable of ... others will no doubt appear here, and in the astronomical literature.

R. F. Carswell
Institute of Astronomy, Cambridge

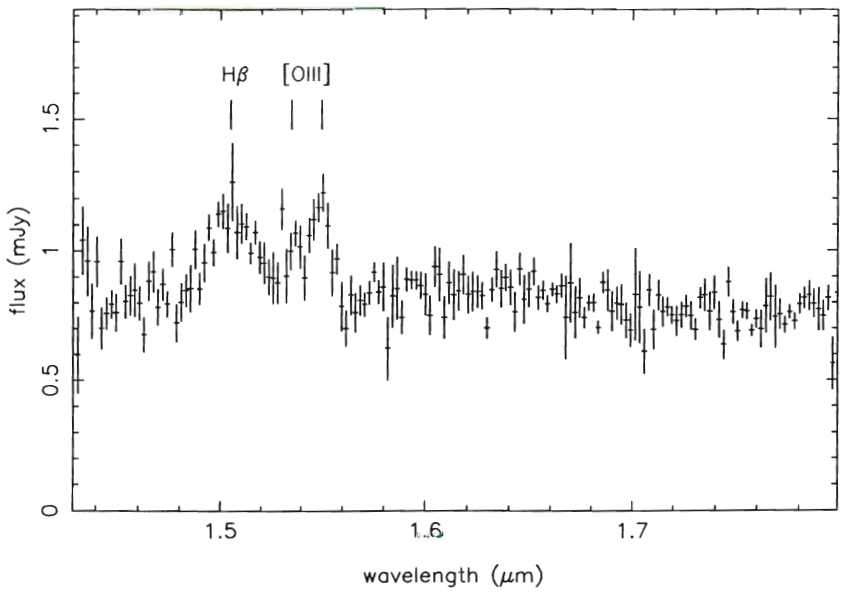

The 1.6μm spectrum of 1331+170, showing the redshifted Hβ and [OIII] emission lines

Neutral Carbon in M42

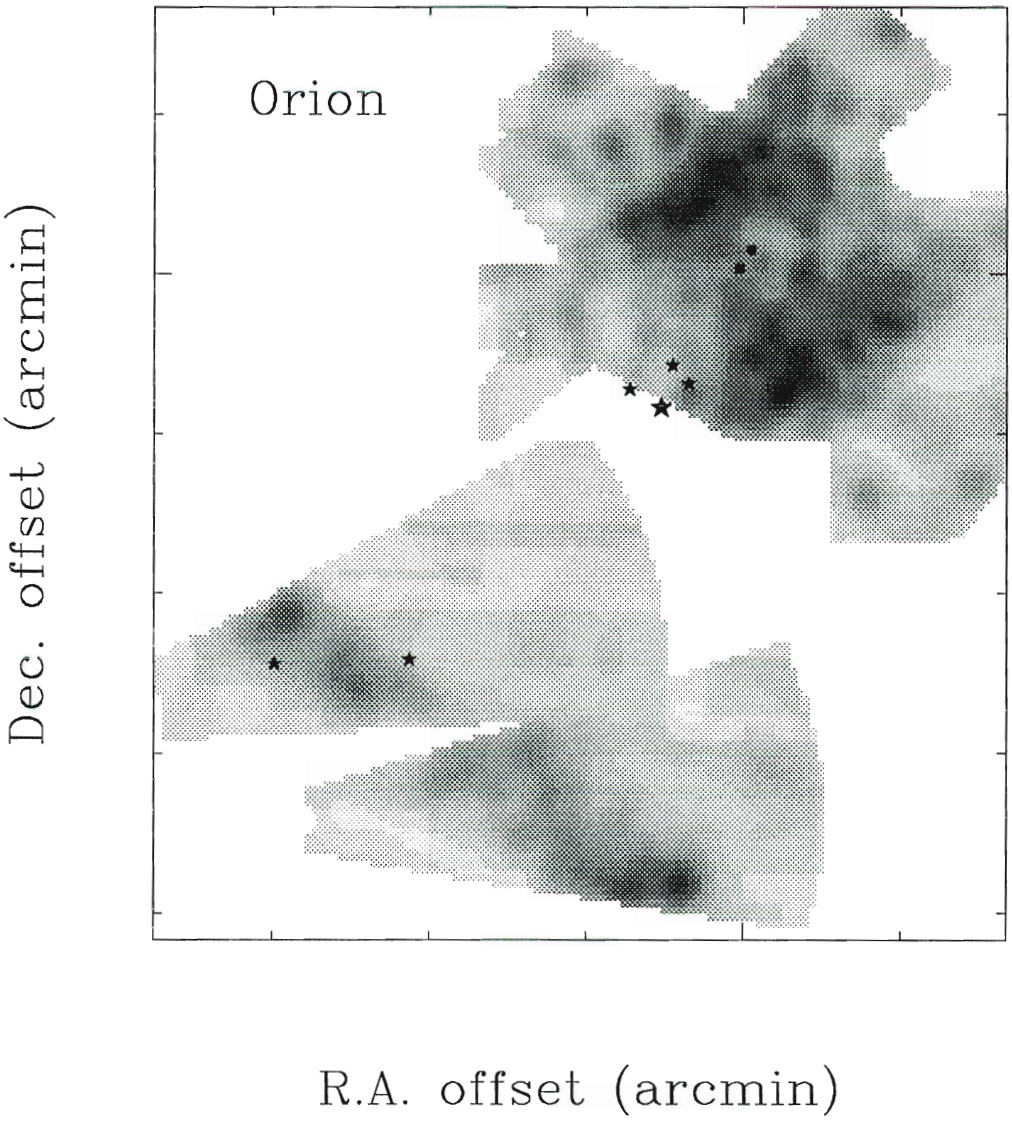

This map of the neutral carbon (CI) emission in **M42**, was obtained at JCMT in April using the common-user receiver C at 492 GHz, by Rachael Padman and Glenn White. The northern region, around the Becklin-Neugebauer object and the Kleinmann-Low nebula, was mapped in a 3 MHz wide passband centered on a *lsr* velocity of 9 km/s; the southern region around the bright bar was centered on 10 km/s. The data were taken in on-the-fly spectral line mode, using azimuth chops of 40 and 150 arcseconds, using the RxC backend. The images were then restored using John Richer's maximum-entropy DBMEM program (see elsewhere in this issue) and displayed using his ANMAPL 2-D plotting and data analysis package. The rather oddly shaped map boundaries arise from source rotation during the time it took to make each Az-El scan.

Salient positions are indicated: BN with a filled circle, IRc2 with a filled square, and the Trapezium cluster (θ-1 Ori) and θ-2 Ori with stars. The cognoscenti will note the wealth of clumpy structure in the IRc2 region, as well as the emission "hole" around BN-KL. The *very* alert will note too that the bright bar lies *between* the two stars of θ-2 Ori, whereas the optical and radio bright bar lies some 30" to the NW, closer to the source of the ionizing radiation.

Rachael Padman (MRAO)
Glenn White (QMW)

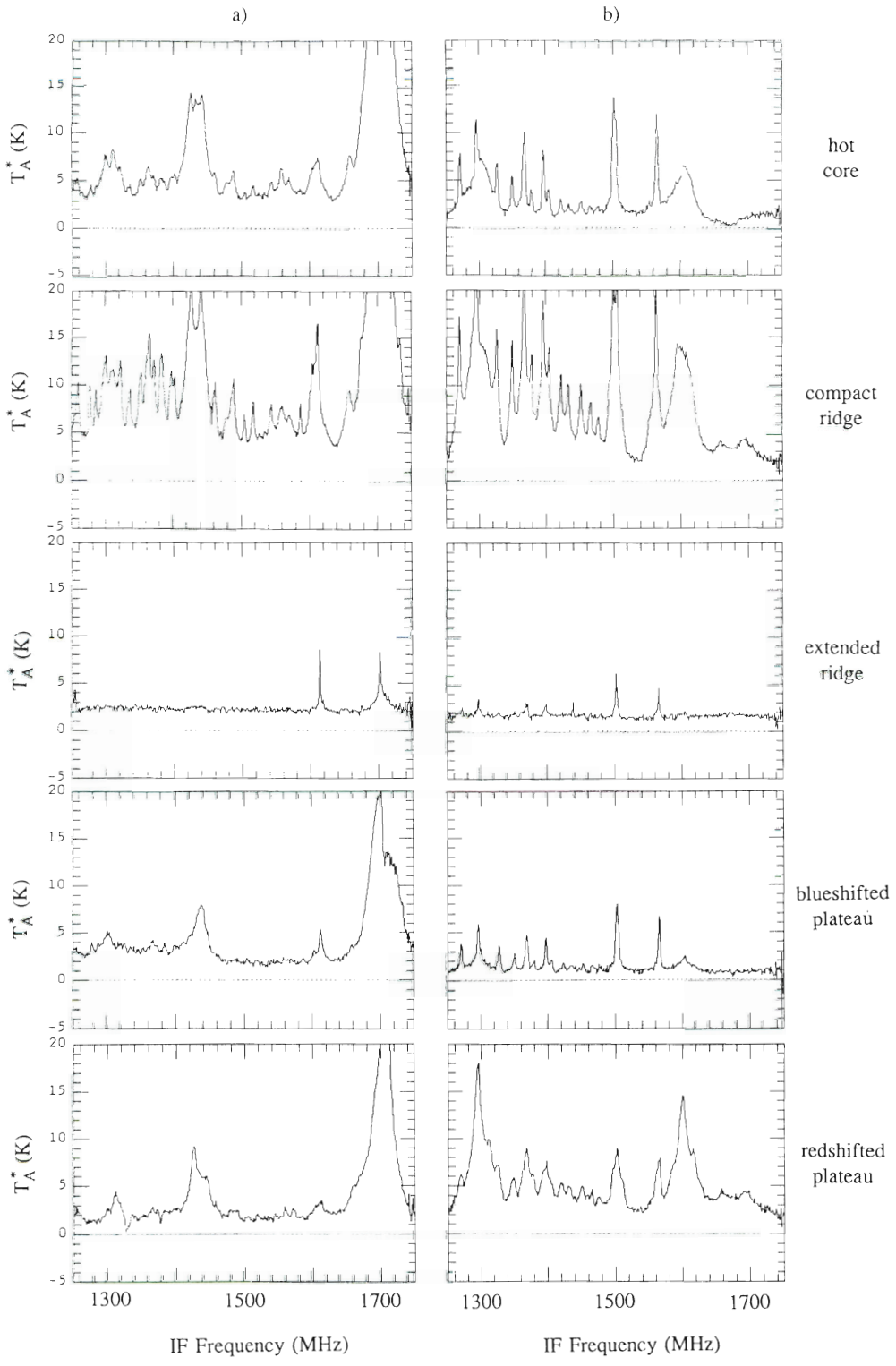

Two sets of spectra from the Orion survey, illustrating chemical differences. Spectra are double sideband, with upper sideband centre frequencies near 340.5 and 341.4 GHz for (a) and (b) respectively. Most of the compact ridge spectra show an extremely dense set of lines, generally leaving no discernable baseline.

Survey of Chemical Differentiation in OMC-1

The Orion nebula is one of the most visually striking astronomical objects. Associated with it is a giant molecular cloud known as OMC-1, a rich collection of gas and dust containing both massive young OB stars and embedded sources thought to be at early stages of stellar evolution. It is the prototypical star forming region. Because of its proximity, it is also one of the most intensively studied molecular clouds.

In recent years it has become apparent that dense molecular clouds can have very rich chemistries, in which large quantities of fairly complex molecular species are formed. In Orion the most complex molecular species observed are CH_3OCH_3 and C_2H_5CN (Sutton *et al.* 1985, Blake *et al.* 1987) and HC_7N (Turner 1991). Molecules such as these, with as many as 9 atoms, are formed via a multi-step process. The relevant reaction network is thought to contain large numbers of gas-phase reactions as well as grain surface reactions. The challenge for theorists is to explain the large observed abundances of complex molecules. In particular, it is important to understand why certain complex species are formed in preference to others and why different molecular clouds have different chemical signatures.

Within the central part of the Orion cloud there are a number of regions representing distinct physical conditions. One of these, which has become known as the "hot core," is a very warm and dense region near the luminous source IRc 2. Another region, known at the "plateau," is characterized by a high velocity outflow thought to originate from IRc 2. The high velocity material is evident via broad molecular line wings and emission from shocked molecular hydrogen in a region where this high velocity flow impacts stationary molecular gas. Quiescent molecular material is present in an "extended ridge" running roughly NE-SW. Near, but somewhat south of IRc 2 and the "hot core", is a "compact ridge," a region of warm dense gas which is kinematically distinct from both the extended cloud material and the other sources near the cloud core. The chemical signatures of these sources vary considerably.

In previous single-dish observations, with large beam widths of order 30" - 2', these sources were observed simultaneously. The contributions of the various components were then distinguished via their kinematics (velocity and linewidth). At submillimeter wavelengths the JCMT provides very high spatial resolution, allowing the sources to be spatially resolved. Near 345 GHz the beam size of the JCMT is 14" (FWHM), comparable to the separation of the various components.

Taking advantage of this unique property of the JCMT, we have undertaken a survey of the molecular emission spectrum from OMC-1. The frequency range surveyed was from 335 to 343 GHz, selected as a region containing lines from a large and diverse set of molecular species. Our approach was to obtain spectra from five positions in rapid sequence, ensuring good calibration and accurate relative pointing. Two such sets of spectra are shown in the figure. The entire data set consists of 41 sets of five spectra each.

One aspect of the data which is most readily apparent is the high density of lines seen at the compact ridge position. The spectra at this position are confusion-limited over much of the range surveyed, with the underlying continuum being completely obscured by overlapping emission lines. This source has a very oxygen-rich chemical composition, with large abundances of CH_3OH, CH_3OCH_3, and $HCOOCH_3$. A number of the lines evident in the figure are associated with the J=7-6 band of CH_3OH.

In further analysis of these data we will be working to derive molecular abundances for all five regions. An important feature of this work is the fact that we observe multiple lines of each species, enabling us to model the molecular excitation and thereby obtain more accurate abundances. This multi-line, multi-species survey will provide some of the best information available to date on the dominant chemical processes in these different regions at the core of the Orion cloud.

E. C. Sutton & P. A. Jaminet
Astronomy Department
University of Illinois
Urbana, Illinois

References

Blake, G.A., Sutton, E.C., Masson, C.R., and Phillips, T.G. 1987, Ap.J., 315, 621.
Sutton, E.C., Blake, G.A., Masson, C.R., and Phillips, T.G. 1985, Ap.J. (Suppl.), 58, 341.
Turner, B.E. 1991, Ap.J. (Suppl.), 76, 617.

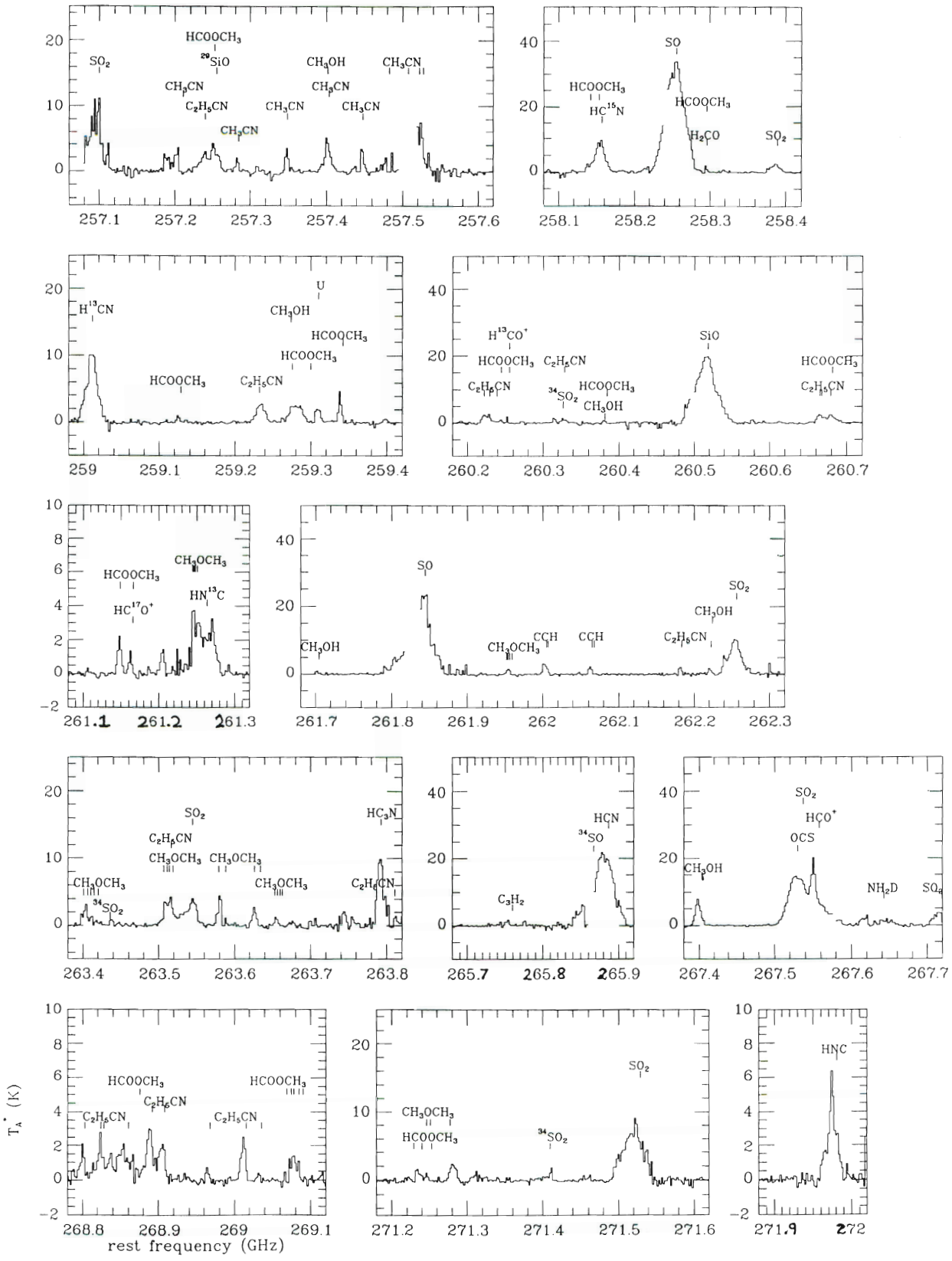

Figure 1. Parts of the 257 - 273 GHz spectrum of the Orion A core. Lines are labelled by molecule; unlabelled features and gaps are artefacts of the algorithm used to deconvolve the original double-sideband spectrum. Drifts in AOS frequency calibration resulted in x-axis errors ≤ 8 MHz.

Chemistry of Orion A: spectral survey and follow-up work

In a previous edition of Protostar (No. 8, September 1989), Glenn White reported preliminary results of our 257-273 GHz spectral survey of the Orion A core, made with the JCMT in 1988. Since then, we have managed to identify all but 4 of the 134 lines detected. A list of the species found, together with the number of transitions of each, is given in Table 1, and the most interesting portions of the spectrum are displayed in Figure 1. The full survey is to be published shortly (Greaves and White, Astronomy and Astrophysics Supplement Series, in press).

With the small beam of the JCMT, the observed line strengths were greater than in previous surveys which included parts of our 257-273 GHz range. This has led to revised abundances for several species, by factors of up to 4. Comparison of these results with chemical models has revealed effects such as varying C/O ratios within the cloud, and the presence of both continuous and jump type shocks in the outflow.

Follow-up observations were made by Nick Parker and myself in 1989, also using the JCMT. The original survey had suggested that C_4H and SiCC, highly reactive radicals with unpaired electrons, were surprisingly abundant in Orion A. However, searches for intrinsically stronger transitions (around 230 GHz) failed to produce any detections, implying the original lines are from still-unidentified species.

An unexpected bonus of the search for radicals was the first detection of CN in the outflow system (Figure 2). Since this species is readily destroyed in collisions, it was previously thought that it could not survive in the dense outflow environment. The abundance of CN is likely to provide a stringent test for chemical models of shocked gas in Orion A.

Jane Greaves
Queen Mary and Westfield College (University of London)

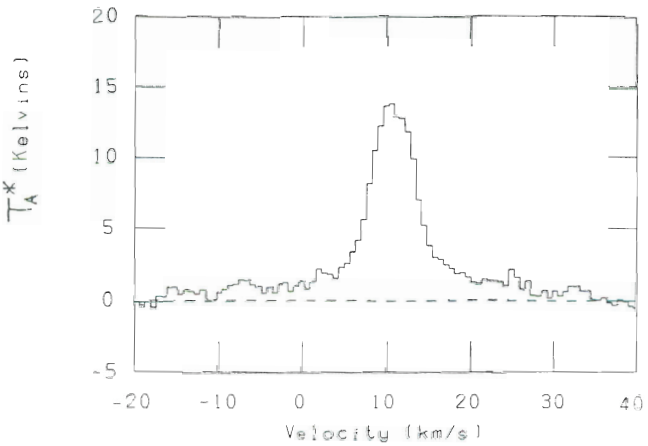

Figure 2. Strongest CN 2→1 hyperfine component, as a position 2" south of the embedded source IRc2 in Orion A. High velocity wings from out-flowing gas are clearly visible. Features at -7 and -15 km/s are additional hyperfines, not outflow material.

Table 1. Number of transitions detected for each species and its isotopically-substituted forms. Some of the transitions are blended together.

SO (3)	SiO (2)	SO_2 (20)	OCS (2)	HCN (3)
HNC (2)	CCH (2)	HCO^+ (3)	HDO (1)	H_2CS (1)
H_2CO (1?)	NH_2D (1?)	HC_3N (4)	CH_2CHO (2)	C_3H_2 (1?)
CH_3CN (11)	CH_3OH (12)	$HCOOCH_3$ (34)	C_2H_5CN (29)	CH_3OCH_3 (18)

Millimetre-infrared observations of Wolf-Rayet stellar winds

Wolf-Rayet stars are luminous, hot stars which lose mass at prodigious rates. Their dense stellar winds form extended ionized envelopes from which free-free emission is observed in the infrared and radio spectral regions. This emission depends on the density, ionization, composition and temperature of the wind and the variation of these with distance from the star. Wright & Barlow (1975) showed that the radio emission from an isothermal wind having an inverse-square density law (i.e. a constant wind velocity) has a spectrum $S\nu \propto \nu^{0.6}$. Most Wolf-Rayet stars which have been observed at more than one frequency in the (cm) radio region have spectral indices close but not equal to 0.6; a few have indices very different from this value owing to additional non-thermal emission processes. The infrared-to-radio spectral indices usually differ from 0.6: either grossly, owing to "excess" infrared radiation from heated circumstellar dust, or subtly, reflecting deviations from the inverse-square density law (the wind is slower nearer the star where the infrared radiation arises) or variations of ionization through the wind. Because the free-free radiation by the wind in the radio and infrared can be masked by additional emission from heated dust or non-thermal processes respectively, and given the huge gap in frequency space between these regions, we have observed the envelopes of Wolf-Rayet stars in the millimetre and sub-millimetre as well. We can then use spectral energy distributions to model density and ionization in the wind and hence the mass loss process.

In March 1991, we used UKT14 on the JCMT to observe the 1100 μm fluxes from a number of Wolf-Rayet stars, including the WN8 star WR 147. This was bright enough to observe at 450, 800, 1300 and 2000μm as well. The fluxes are plotted

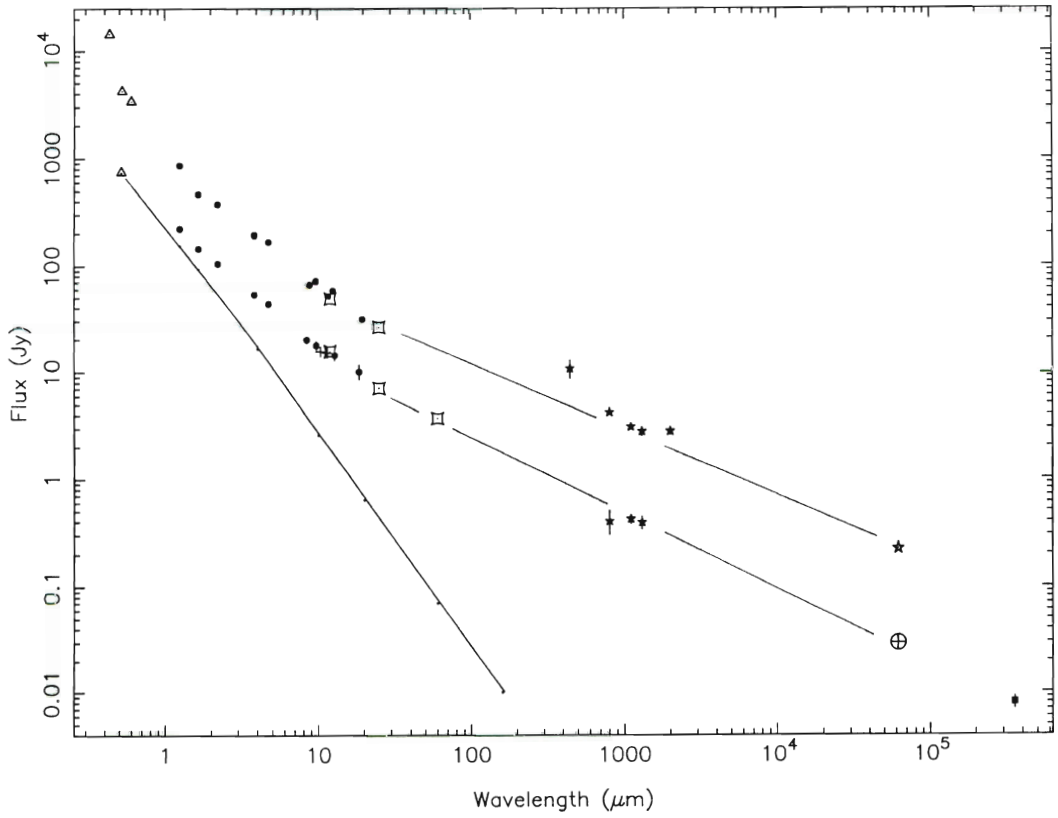

Spectral energy distributions of WR 147 (top, x10 for clarity) and γ Velorum. The filled circles represent fluxes from ground-based photometry from UKIRT and ESO respectively; the open squares from IRAS data corrected for the power-law spectra. The radio flux for WR 147 is from Moran *et al* and those for γ Vel from Hogg (1985) and Jones (1985); earlier single-dish observations of γ Vel are contaminated by the nearby source 0808-471. The line fitted to the optical photometry of γ Vel is the spectral energy distribution of a stellar photosphere for comparison.

in the figure, together with fluxes derived from infrared photometry with UKIRT (UKT6 and UKT7 in 1983; UKT9 in 1990) and IRAS. The infrared (and optical) data have been corrected for interstellar reddening. The radio flux is the MERLIN observation by Moran et al. (1989) of the southern radio component, which they identified with the optical image of the star.

The 800, 1100 and 1300μm fluxes are consistent with the $\nu^{0.6}$ infrared-radio spectrum; the 450μm and 2mm fluxes were observed on one night and need to be confirmed. If true, additional observations at shorter and longer wavelengths will be required. The UKT14 beam included the non-thermal radio component 0".6 north of the star but it would be surprising (from the level of the cm flux) if this contributed significantly at 2 mm. The $\nu^{0.6}$ spectrum from the infrared longward shows that the wind has accelerated to its terminal velocity within a few stellar radii from the star, where the infrared continuum arises, and that recombination in the wind must also occur within this region.

This is in contrast to the continuous spectrum of the WC8 star γ Velorum, also plotted in Figure 1. The infrared-millimetre-radio spectral index is 0.70, significantly steeper than 0.60. This was interpreted in terms of continued recombination in the wind at about 100 R* from the star (Williams *et al.* 1990). It is not certain why the WC8 stellar wind should recombine much further from the star than the WN8 wind. More precise determination of the continuous spectra of these stars using millimetre observations are needed.

Karel A. van der Hucht
SRON Space Research Laboratory, Utrecht

Peredur M. Williams,
Royal Observatory, Edinburgh

Diah Yudiawati Anggraeni
Astronomy Department, Institute of Technology, Bandung, Indonesia.

References

Moran, J.P., Davis, R.J., Bode, M.F., Taylor, A.R., Spencer, R.E., Argue, A.N., Irwin, M.J. & Shanklin, J.D., 1989. Nature, **340**, 449.

Williams, P.M., van der Hucht, K.A., Sandell, G. & Thé, P.S., 1990. MNRAS, **244**, 101.

Wright, A.E. & Barlow, M.J., 1975. MNRAS 170, 41.

CO J=6→5 Observations of Low Mass Star-forming Regions

This research report describes the first CO 6→5 observations of low mass star-forming regions, part of an ongoing project using RxG on the JCMT. It is no longer a big surprise to find large amounts of warm dense gas associated with regions of high mass star-formation. This project seeks to investigate the physical properties of the gas around low mass stars. Since the J=6 level of CO is about 115 K above ground, we initially wanted to study emission from subthermally excited material which is very sensitive to the physical conditions of the gas. However the 6→5 lines have turned out to be strong, and as with mm lines, we will have to use rare isotopes to really extract the physical conditions of the gas.

Observations of low mass stars have only recently become possible because of the combination of the sensitivity of RxG and the improving surface of the JCMT. Using Jupiter we measured an efficiency of 0.2 (η_{fss}* η_{tel}) in July and 0.24 in December after adjustment of the surface.

The data were taken during runs in July 1990 and December 1990. The July run was the most remarkable RxG campaign to date. We were fortunate enough to hit a period of super-dry weather and observed continuously around the clock some 60 hours, about 30 of which had a remarkable 50% transmission at zenith.

Results

The table shows the results for all the sources observed. Because of the limited space available here, we will not discuss all of these sources, but will concentrate on a few specific examples.

B335

B335 is an archetype isolated core containing an embedded source with a total bolometric luminosity of 3 $L_\odot$. We have made a 6-point map in CO 6→5 and have a single ^{13}CO 6→5 spectrum at the 0,0 position (figure 1). The deconvolved source size from the 6→5 map is about 8 arcsec. Once we have a source size estimate, it is possible to calculate the gas kinetic temperature assuming that the ^{12}CO line is optically thick. This give a Planck-corrected kinetic temperature of 39 ± 10K. The error quoted here comes mainly from the uncertainty in correction for the source coupling correction. The result is in good agreement with the 31K calculated by Chandler et al. (1990).

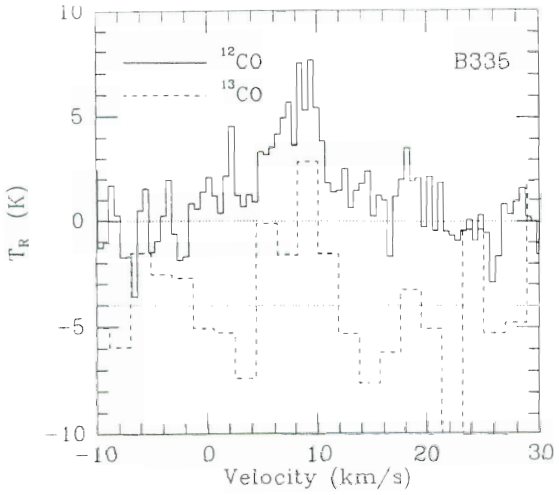

Figure 1. ^{12}CO (solid line) and ^{13}CO (dashed line) 6→5 spectra of B335

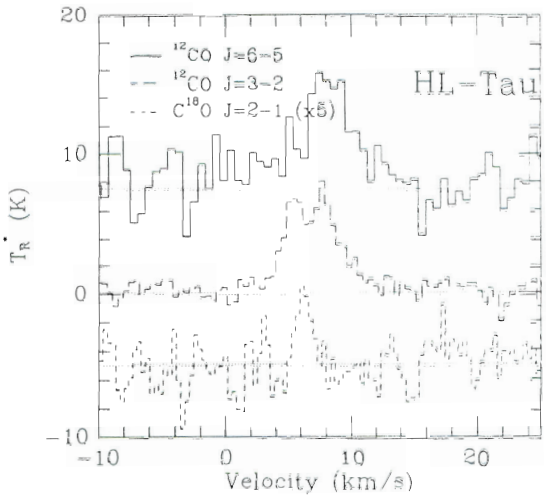

Figure 2. ^{12}CO 6→5 spectrum of HL Tau overlaid on ^{12}CO 3→2 (dashed line) and C^{18}O 2→1 (dotted line)

Although the ^{13}CO spectrum is a marginal detection, it is clear that it is about as bright as the ^{12}CO line. This means that even ^{13}CO is optically thick in B335. Adopting a limit of $\tau \geq 2$ implies a ^{13}CO column density of $N(^{13}CO) \geq 3 \times 10^{17}$ cm^{-2} or $A_v \geq 280$. For an 8 arcsec source size, this corresponds to a mass ≥ 0.4 $M_\odot$ and a volume averaged density of $n \geq 10^7$ cm^{-3}. It is very unusual to calculate such a high volume density directly from molecular line observations. This is probably why the dust and gas temperatures agree so well, indicating that at such densities, the dust and gas are well coupled thermally.

6→5 Observations of low mass star-forming regions

Source	TR*	dV	L_{bol}	T_{rad} #	comments
B335	5.4	7.2	3	50	^{13}CO=4.9K
L1262A	6.0	5.1	1	50	
L43	4.4	2.8	4	64	
L1551	8.0	6.0	25	76	
IRAS 16293	23.3	10.3	27	76	Self absorbed
NGC 1333-IRAS1	8.6	20.7	70	83	Self absorbed
WL16	<4.0		16	70	3 sigma limit
WL21	<4.5		10	70	3 sigma limit
Elias 29	5.3	7.2	20	74	
T Tau	24.2	5.0	56	77	
HL Tau	7.8	4.6	10	79	
GG Tau	<10.0				3 sigma limit

Dust temperature 4 arcsec from source assuming a spherical dust cloud radiatively heated from within.

T-Tauri stars

In HL Tau we have made a 6-point map in CO 6→5. The central position is shown in figure 2 overlaid on C^{18}O 2→1 and ^{12}CO 3→2. Both the 6→5 and the 3→2 lines show a systematic red-shift from the quiescent cloud. Over the region we have mapped, the red-shifted emission dominates to the south west - in the same direction as the red-shifted optical jet in HL Tau. The CO 3→2 line shows strong self absorption. We believe that the absorbing material has completely removed the quiescent component of the 6→5 spectrum, leaving only the red-shifted component. This is plausible since the HL-Tau system is viewed roughly edge on through an extended cloud or disk, whereas T-Tau is seen more or less pole on and shows little or no absorption of the 6→5 line. An escape probability analysis of the 6→5 to 3→2 line ratio gives a gas kinetic temperature of about 150K and a CO column density of 3×10^{16} cm^{-2}.

T-Tau shows unexpectedly bright ^{12}CO 6→5 emission (figure 3). We have made a 7-point map which gives a deconvolved source size of 5.5 - 8 arcsec. This gives a source size corrected kinetic temperature of 150 ± 50K. The lower limit to the mass, assuming that ^{12}CO is optically thin, is a few thousandths of a solar mass. We hope to get the ^{13}CO line this winter which will allow an accurate determination of the mass of hot gas in T-Tau.

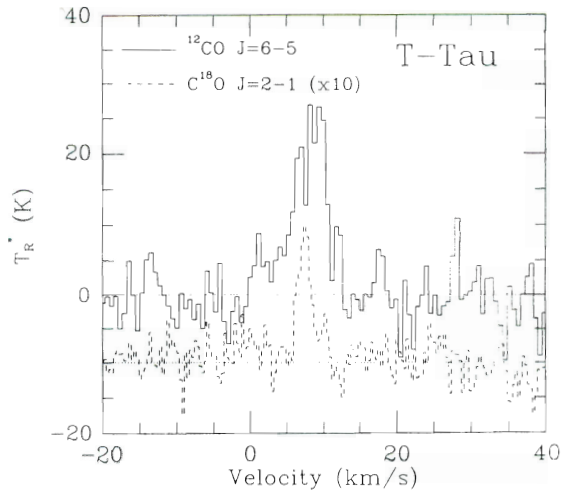

Figure 3. ^{12}CO 6→5 spectrum of T Tau overlaid on C^{18}O 2→1

Discussion

One possibility to account for the gas temperatures in the embedded sources is by simple radiative heating of a spherical dust cloud (eg Emerson 1988). Column 5 in the table shows the dust temperature at a projected radius of 4 arcsec for radiative heating and a $\beta = 1.5$ dust emissivity law. Since we have estimated volume densities in excess of 10^7 cm^{-3}, the gas will be well coupled thermally to the dust. It is clear however from the large observed linewidths that we are not seeing quiescent material. In all the embedded sources we expect ^{12}CO 6→5 to be very optically thick. This means that we are probably seeing the outer parts of the cores surrounding these young objects. However accretion is unlikely to be responsible for the large linewidths - the model of isothermal collapse by Shu (1977) predicts that an infall velocity of 1 km/s is only reached 10^{16} cm from the star (5 arcsec @140 pc). Higher velocities appear only on much smaller scales. It seems likely therefore that the increased linewidth is in some way associated with the outflows from these objects. We see direct evidence for outflow in IRAS 16293, NGC 1333-IRS1 and HL Tau. In the other sources however, the lines are wide but Gaussian. It is possible that the cores are being disrupted by their outflows, resulting in an increase in the turbulent linewidth. This suggests that shock heating may be important. Another interesting feature is that the spectra of the embedded sources are mostly not self-absorbed. We hope to use this to place constraints on the physical conditions in the outer envelopes of the cores.

In the T-Tauri stars we cannot explain the 150 K gas temperatures by radiative heating. It is also clear that we cannot be seeing the compact 100 AU disks seen in the continuum because beam dilution would be too great. Thus models of viscous heating in active disks cannot help at this scale unless the disks are really 1000 AU in diameter. Large "disks" have been reported around T-Tau and HL Tau from interferometric observations (Weintraub *et al.* 1989, Sargent & Beckwith 1987). However these "disks" are too cold and have too small a linewidth to explain our observations. The other obvious possibility is shock heating. Present shock models, however, cannot reproduce the observed 6→5 line flux from a 5 km/s shock. Thus unless we have many optically thin shocks in our beam, or have very oblique shocks, the high gas temperatures seen around T Tau and HL Tau remain a mystery.

Acknowledgements

The successful operation of RxG on the JCMT has only been possible due to the effort of many people who have worked to bring the telescope to its present state. We would particularly like to thank both the day and night crews who worked so hard in July to permit our marathon observing session.

Adrian Russell
JAC

Karl Schuster, Nels Anderson, Reinhard Genzel, Urs Graf, Andrew Harris & Juergen Stutzki,
Max Planck Institute for Extra-terrestrial Physics.

References

Chandler C.J., Gear, W.K., Sandell, G., Hayashi, S., Duncan, W.D., Griffin, M.J. Hazell, A.S., 1990. MNRAS 243, 330.

Emerson, J.P., 1988. in NATO-ASI on "Formation and evolution of Low Mass Stars", ed. A.K. Dupree and M.T.V.T. Lago (Dordrecht: Reidel).

Sargent, A.I. and Beckwith, S., 1987. ApJ 323, 294.

Shu F.H., 1977. ApJ 214,488.

Weintraub, D.A., Masson, C.R. and Zuckerman, B., 1989. ApJ 344, 915.

Compact high-density gas disks in bipolar outflow sources - Results from a survey in $H^{13}CO^+(J=4\rightarrow3)$

We present a brief look at a survey of $H^{13}CO^+(J=4\rightarrow3)$ emission in bipolar outflow sources performed by a collaboration between the JCMT and our group at the University of California at Berkeley. For this work we used a high-sensitivity SIS (superconductor-insulator-superconductor) tunnel junction receiver system (developed by our group; cf. *Sutton et al.*, 1990) for the atmospheric window around 345 GHz. The observations were made at JCMT in March 1990.

The radical HCO^+ requires relatively high critical densities of hydrogen for collisional excitation, i.e. $N_{crit} \geq 10^6$ cm^{-3}. This is related to its large permanent electric dipole moment (2.5 Debye compared to 0.11 Debye for CO) which substantially increases its Einstein A-coefficient compared with CO for example. Because it is a product of the ion-molecule chemistry which takes place in dense interstellar clouds, it is commonly seen (cf. *Blake*, 1985 for more information on molecular cloud chemistry), and is often used as a tracer of dense gas in such clouds. The isotopic partner of HCO^+, $H^{13}CO^+$, was chosen on the basis that it was not likely to be optically thick.

Discussion

The sources for this survey were chosen to cover a large range in luminosity as can be seen in the Table. Luminosities vary from ~8$L_\odot$ for B335 up to ~2×10^5 $L_\odot$ for NGC 6334I-IRS 1. The morphologies of the outflows vary widely as well. For example, the axis of the lobes of the outflow for S140 is nearly along the line-of-sight, whereas for B335 and L1551 the outflows are more nearly perpendicular to the line-of-sight (cf. *Bally and Lada*, 1985, and *Lada*, 1985).

The majority of the observations were made using the chopping secondary with typical throws of 150-200 arc seconds in azimuth at a frequency of 1 Hz. Position switching was used for the remainder of the observations with similar offsets between on-source and off-source positions. The spectra were calibrated by the chopper-wheel technique in which the ratio of the spectrum of the source minus the sky to the spectrum of an ambient temperature load minus the sky is taken. The antenna temperature T_A^* is this ratio times an effective temperature for the atmosphere (cf. *Penzias and Burrus*, 1973, and *Kutner and Ulich*, 1981).

Because of space limitations for this paper we will discuss the data only briefly. Table I summarizes the results. First, note that $H^{13}CO^+(4\rightarrow3)$ emission is observed from *all* the sources. Second, a rough calculation of the integrated intensity of the lines (i.e., $T_A^*\Delta V$) gives the result that the integrated intensity increases with the luminosity of the

Table of $H^{13}CO^+$(4-3) Observations

Source	RA(1950)			DEC(1950)			T_{A*}(1)	ΔV	V_{LSR}	Luminosity (2)
	h	m	s	o	'	"	K	kms^{-1}	kms^{-1}	$L_\odot$
GL 490	3	23	39.22	58	36	35.6	0.5	3.0	-12.	1.4×10^3
SSV 13	3	25	58.14	31	5	45.0	0.8	1.5	+9.0	5.8×10^1
L1551-IRS 5	4	28	40.24	18	1	42.1	0.4	1.5	+7.0	3.8×10^1
NGC 6334I-IRS 1	17	17	32.33	-35	44	3.11	2.0	6.0	-6.0	2×10^5
B335	19	34	34.7	7	27	15.0	1.0	1.0	+9.0	8.0×10^0
DR 21	20	37	14.0	42	09	00.0	1.9	6.0	-4.0	1.5×10^5
LkHα 234	21	41	57.1	65	53	9.0	0.4	2.0	-9.0	1.0×10^3
S140	22	17	42.06	63	03	41.7	2.0	3.0	-7.0	2×10^4

(1) Here T_{A*} are calibrated by the chopper-wheel technique, but do not include corrections for beam efficiencies.
(2) Luminosities are from *Bally and Lada*, 1983 and from *Sandell*, 1989.

source. Third, in at least two of the "classical" low luminosity sources, B335 and L1551, the emission was found to be unresolved, which supports the view that the star driving the outflow is surrounded by a compact disk of very high density. The sources SSV 13 and GL 490 may also be unresolved, but we were unable to map them because they were daytime objects during our observing run. For the intermediate and high luminosity sources the dense material surrounding the stars is much more extended, and we obtained fully-sampled maps of S140, DR21 and NGC 6334I. Thus we will be able to determine if $H^{13}CO^+$ traces the morphology of the disks that are expected to surround these objects. It is also interesting to see if we can obtain better information abut the dynamics of these disks by using a line that is optically thinner than is typically used to probe disk emission, *e.g.*, CS(2-1). We will also be able to make comparisons with the geometry of the CO outflows. (A larger sampling would be desirable, but limitations of observing time precluded that.) Fourth, an unexpected bonus was discovered in the spectra for NGC 6334I, where more than twenty molecular lines were observed within the IF passband of the receiver, as can be seen in Figure 1. It appears that only $H^{13}CO^+$ is extended; all the other lines seem to come from an unresolved source, indicating they are all high-excitation lines. It is possible that NGC 6334I is as rich in molecular lines as OMC-1 and SGR B2, and since the lines are narrower than in OMC-1, it may be an excellent source in which to search for new molecular species. Finally, very rough estimates of the column density of $H^{13}CO^+$ can be made from the integrated intensity ($T_{A^*}\Delta V$). The total column density of $H^{13}CO^+$ ranges from 10^{12} cm^{-2} to above 10^{13} cm^{-2}. Additional work is in progress to understand the data in detail and additional publications will be forthcoming.

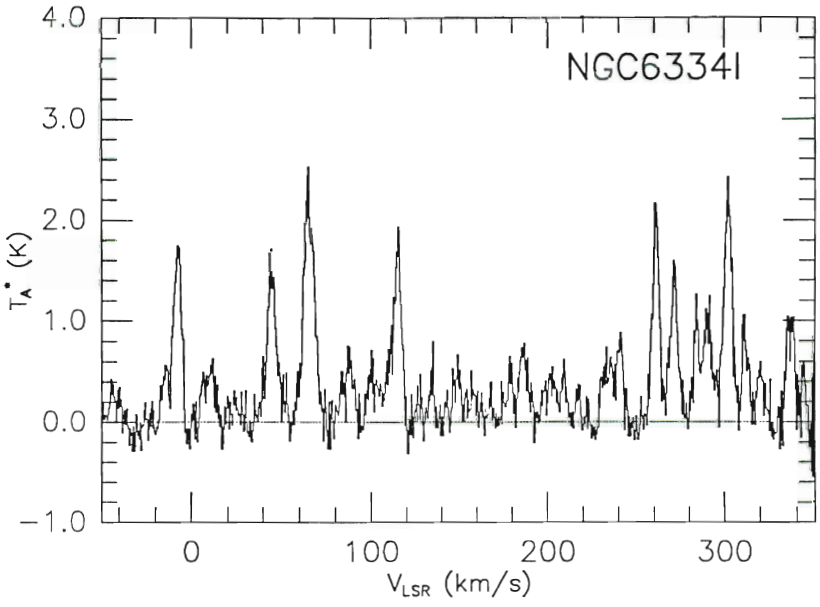

Figure 1 Spectrum of NGC 6334I. Which of the many lines is from $H^{13}CO^+(4\rightarrow3)$? Using the LSR velocity for NGC 6334I in the Table we can see it is the rather typical looking line at -6km/s. Our maps show that as soon as we move away from the strong continuum source, all the lines disappear except $H^{13}CO^+$, which demonstrates its ability to trace the cold dense material surrounding the source.

Acknowledgements

The collaboration included G. Sandell of the JCMT, A.P.G. Russell (formerly of the JCMT, now at the MPIfEP in Garching), and E.C. Sutton and P.A. Jaminet (both formerly at U.C. Berkeley, now at the University of Illinois at Urbana-Champaign).

This work has been supported in part by a grant from the National Science Foundation, AST88-18327, and the author also has been supported in part by the L.W. Frohlich Research Fellowship of the New York Academy of Sciences.

William C Danchi
University of California,
Berkeley, USA

References

Bally, J. and Lada, C., 1983, *Ap.J.*, **265,** 824.

Kutner, M.L. and Ulich, B.L., 1981, *Ap.J.*, **250,** 341.

Lada, C., 1985, *Ann.Rev.Astr.Ap.*, **23,** 267.

Penzias, A. and Burrus, C., 1973, *Ann.Rev.Astr.Ap.*, **11,** 51,

Sandell, G., 1989, Kona Conference.

Sutton, E.C., Danchi, W.C., Jaminet, P.A. and Ono, R.H., 1990, *Int.J.IR and Millimeter Waves,* **11,** 133,

Solid Carbon Monoxide studied with CGS4

The nature and evolution of interstellar dust, and its significance as an active ingredient of the interstellar medium regulating both physical and chemical processes, are key problems in modern astrophysics (see refs. [1] and [2] for comprehensive reviews). Infrared spectroscopy provides particularly valuable diagnostics of the composition and evolution of interstellar grains and the quantitative impact of mantle growth on gas--phase abundances [e.g. 3].

Condensation of grain mantles in molecular clouds has dramatic consequences for models of cloud chemistry [4,5]. Grain surfaces provide sources and sinks for gas phase atoms and molecules, and sites for chemical evolution as grain material is recycled during star-formation processing. Laboratory results [6] demonstrate the value of IR spectroscopy for investigating the composition and thermal history of grain mantles. For example, the position, width and profile shape of the 3.0 micron water-ice and 4.67 micron solid CO features are sensitive to the composition and degree of annealing of the molecular matrix in which the absorber is contained [7, 8]. In combination with observations of gas-phase column densities, the solid CO feature gives vital quantitative information on the depletion of this key molecule [9, 10], thus constraining models for mantle desorption in dark clouds [11].

In a four-night "shared-risks" run with CGS4 in May, the 4.67μm solid CO absorption was observed in lines of sight through the Rho Ophiuchi and Serpens dark clouds. It was found that the optimum observing mode for work in the M (4-5μm) band is to periodically nod the telescope through a distance of one chopper throw along the CGS4 slit; this gives a usable quick-look spectrum when observing in the presence of rapid sky-emission variations and thermal beam imbalances. An example of a raw image is shown in Figure 1. The continuum source is VS17 - an embedded object in the Rho Oph cloud. The wavelength scale runs from 4.55 to 4.95 μm; solid CO absorption is plainly visible between 1/3 and 1/4 of the way from the lefthand side of the frame. Since we were both chopping and nodding, there are three spectra here: one "positive" and two "negative" spectra of half-intensity. A slight ripple along the dispersion direction (left-right) is caused by sky variations between array translation positions. It should be possible to remove this effect by straightforward sky-subtraction; at present it appears that this may not be as simple as it sounds.

Spectra can be extracted from the "reduced group" frames using standard FIGARO almost as one would handle optical CCD frames. Figure 2 shows a finished article - summing the three sky-subtracted spectra (remembering to invert the two "offset-beam" spectra before doing so !). Previous observations (with CGS2) had failed to match the feature in VS17 to any known laboratory mixture. The spectrum obtained with CGS4 has a S/N of around 30, representing a great improvement; as an

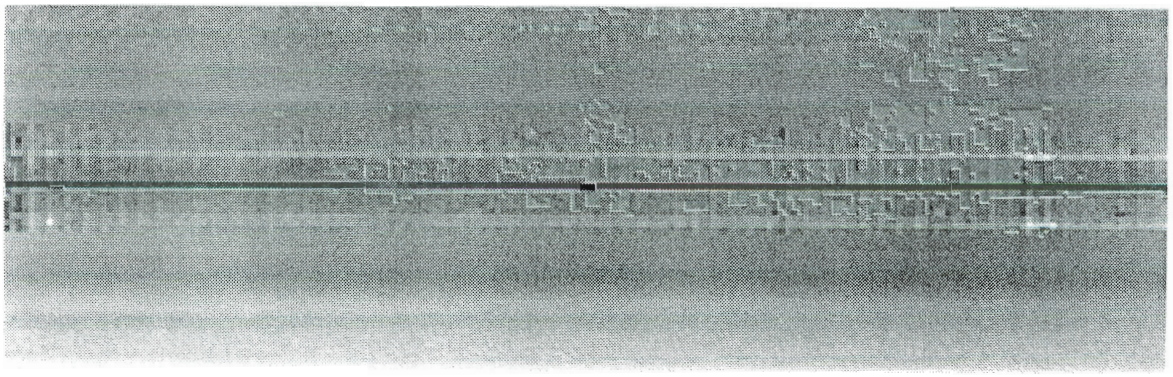

Figure 1. An example of a 'raw' flat-fielded and atmosphere-corrected image from the CGS4 on-line data reduction system. It shows the three M spectra obtained by chopping and nodding the single continuum source, VS17, up and down the CGS4 long slit.

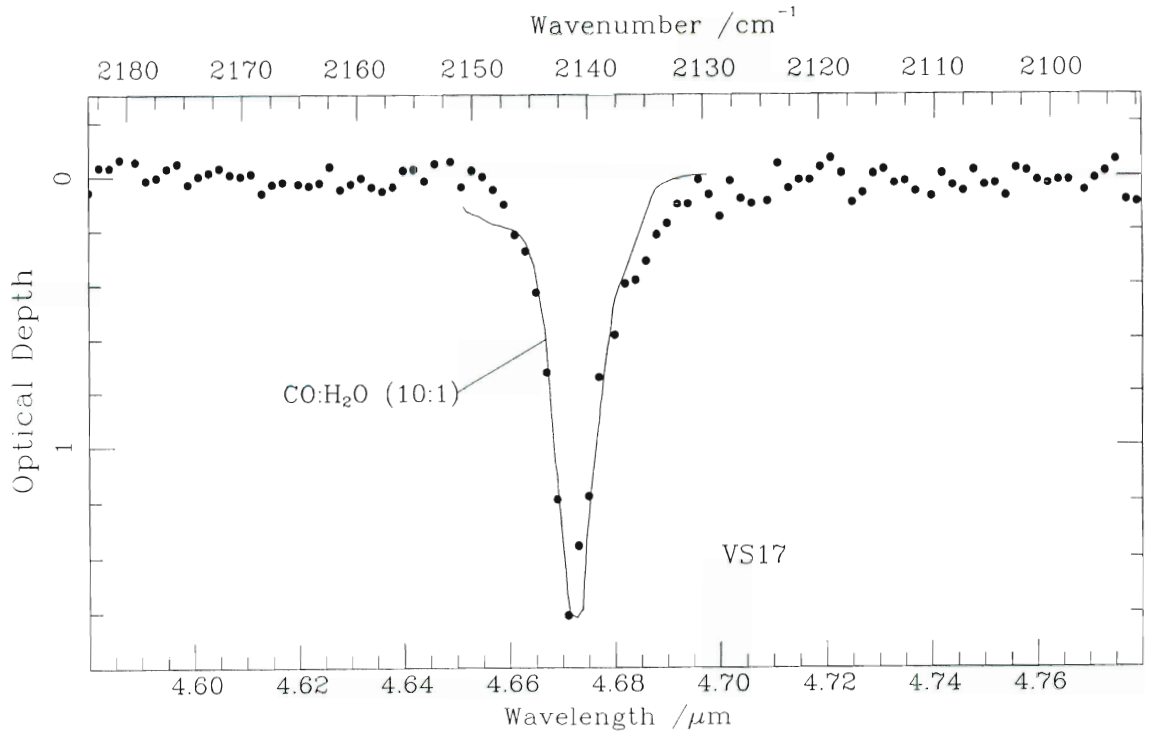

Figure 2.

illustration of the potential of these data for modelling, superposed on the VS17 spectrum is the spectrum of a realistic CO:water-ice mixture, computed for typical grain sizes using laboratory measurements of the bulk optical constants [12].

With observational information of such high signal-to-noise and reproducibility, it will be possible to model the profiles of CO and ice features and determine almost unambiguously the other major constituents of grain mantles; CGS4 promises to be a world-beating source of such data.

Andy Adamson & Tom Kerr
Lancashire Polytechnic

Doug Whittet
Rensselaer Polytechnic Institute, N.Y.

References

[1] Bailey and Williams (eds.) 'Dust in the Universe', C.U.P. (1988).

[2] Allamandola and Tielens (eds.) Interstellar Dust, Kluwer Press (1989).

[3] Whittet, in 'Dust in the Universe' p. 25 (1988).

[4] Williams, in 'Physical Processes in Interstellar Clouds', p. 377, Reidel (1987).

[5] d'Hendecourt *et al.*, Astr. Astrophys. 152, 130 (1985).

[6] Allamandola and Sandford, in 'Dust in the Universe', p. 229 (1988).

[7] Smith *et al*, Astrophys.J., 344, 413 (1989).

[8] Sandford *et al*, Astrophys.J., 329, 498 (1988).

[9] Whittet *et al*, Mon.Not.R.astr.Soc. 241, 707 (1990).

[10] Whittet & Duley, Astr.Astrophys.Rev. (1990, in press).

[11] Duley *et al*, Mon.Not.R.astr.Soc. 241, 697 (1989).

[12] Tielens *et al.* 1991 preprint.

Dust Around Pre-Main-Sequence Stars

One of the great pursuits of astronomy is to learn more about how the Earth and planets formed and to determine the likelihood that other planetary systems can form, have formed and are forming elsewhere. While detections of extrasolar planets remain at or beyond the edge of our current technological skills, with JCMT we can study the environments of pre-main-sequence stars around which planets may now be forming. These studies could reveal information about the commonness of planetary systems, the timescale for accretion of planets, and the efficiency of planet formation.

Our studies have used new observations in sub-mm and mm continuum passbands and have focused on three types of pre-main-sequence stars: classical T Tauri stars (cTTs), FU Orionis stars (FUors) and Herbig Ae/Be stars (HBes). T Tauri are low mass ($< 3\ M_\odot$) pre-main-sequence stars representative of our Sun when our solar system was forming, five billion years ago. Similarly, the circumstellar environments of T Tauri stars are representative of our planetary system during the epoch of planet building. FUors are a subclass of T Tauri stars, characterized by a rapid (few months) and dramatic (up to six magnitudes in the visible) increase in luminosity. This burst has been explained as an evolutionary phase during which the accretion rate from a hot, optically thick disk onto the central star is very high, perhaps as high as 10^{-4} solar masses per year (Hartmann *et al.* 1989). In contrast, estimates of accretion rates for classical T Tauri stars are smaller by 3 to 5 orders of magnitude. HBes are early type emission line stars thought to represent intermediate mass ($< 10\ M_\odot$) equivalents of T Tauri stars.

The canonical model of planet formation assumes that protostellar nebulae collapse quickly to form central masses surrounded by flattened accretion disks. These disks feed the growing stars, collimate bipolar molecular outflows and offer environment favourable for the formation of planetesimals. Traditional thought also suggests that the size of these circumstellar disks will be of order 100 AU, the size of our own planetary system. In addition, astronomers generally have assumed that these disks are optically thin at sub-mm and mm wavelengths and therefore that the masses of relatively unevolved disks can be estimated from observations of thermal emission from dust grains in this wavelength regime.

Our investigations have focused on evaluating several of these assumptions. We have measured the long wavelength spectral energy distribution (SED; Jy x Hz) for a large number of cTTs, FUors and HBes by observing each source in at least three continuum passbands between 350 μm and 2 mm. From the slope of the SEDs, and from models that include data from IRAS and/or the Kuiper Airborne Observatory, we are able to evaluate whether some of the sources are optically thick or thin in the sub-mm. We also have used five-point routines to roughly measure the 800 μm size of many sources and we have demonstrated that the five-points do provide dependable estimates as to whether sources are extended relative to the Gaussian size of the 800 μm beam ($13.5" < \text{HPBW} < 16"$, depending upon the selected aperture). In addition, we have made diffraction limited (7.5" - 8") maps at 450 μm of selected sources. The five-points and the 450 μm maps allow us to test two assumptions: first, whether the morphologies of the long wavelength emission sources are disk-like, and second, whether the thermal sources are small enough to be considered point-like or are large enough to suggest structures larger than 100 AU disks.

Results

We have conducted a survey of 31 cTTs including eight FUors or possible FUors, and 20 HBes (Weintraub, Sandell and Duncan 1989, 1991a,b; Sandell, Weintraub and Duncan 1991). The observed sources were selected primarily on the basis of their having the largest IRAS flux densities among these classes of pre-main-sequence stars and IRAS colors most indicative of large amounts of warm circumstellar dust (Weintraub 1990). Only six of the cTTS escaped detection; all of the FUors and 12 of the 20 HBes were detected. These results suggest that the far-infrared SEDs can be used to predict the sub-mm thermal continuum; however, in many cases the measured sub-mm flux densities were significantly larger or smaller than predicted, under the assumption that the source is optically thin beyond 100 microns and that the long wavelength SED falls off in proportion to the fourth or fifth power of the frequency, where the Planck function, in the Rayleigh-Jeans regime, is modified by the frequency dependent dust grain opacity ($\propto (\text{frequency})^\beta$, where $1 < \beta < 2$).

The cTTs T Tauri ($\beta = 0.7 \pm 0.1$; d = 140 pc), HL Tauri ($\beta = 0.6 \pm 0.1$; 140 pc) and DG Tauri ($\beta = 0.2 \pm 0.2$; 140 pc), the FUors Z CMa ($\beta = 0.16 \pm 0.20$; 1150 pc), V1331 Cyg ($\beta = 0.4 \pm 0.4$; 700 pc) and FU Ori ($\beta = 0.56 \pm 0.50$; 460 pc),

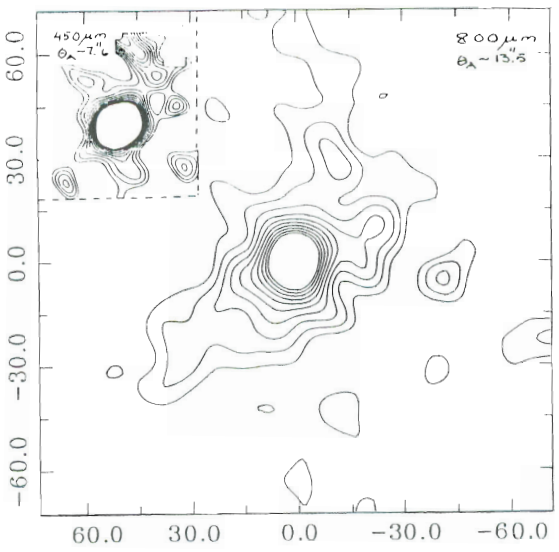

Figure 1. Contour plot of the 800 μm dust emission surrounding LkH-α 234. Inset in the upper left hand corner is a high resolution 450 μm map of the central 40" x 40" area surrounding the star. Although the 800 μm map indicates that the stars is located in a ridge of extended emission, we can see from the 450 μm map, that we have managed to resolve the emission from the star into a marginally disk like compact source of ~ 5.8" in size (from Sandell, Weintraub, and Duncan 1991).

and the HBes AB Aur ($\beta = 0.53 \pm 0.38$; 140 pc) and LkH-α 198 ($\beta = 0.74 \pm 0.49$; 600 pc) all have β indexes significantly below unity. The Kramers-Kronig relation requires $\beta > 1$ for an isothermal population of dust grains; however, such shallow spectra could be produced from the superposition of spectra from grain populations with different temperatures (Casey and Harper 1990). In fact, circumstellar disks, heated by a central pre-main-sequence star, would impose just such a temperature distribution. The slope of the sub-mm SED therefore may provide evidence that demonstrates these stars are surrounded by disks. Of course, if the effective β values are evidence for disks with temperature gradients, then submillimeter flux densities and an apparent (or assumed) beta index cannot be used to directly calculate the mass of the dusty nebulae. Instead models, such as those developed by Adams, Lada and Shu (1988) for disks described by temperature, density and emissivity gradients, must be used in order to determine the structures of the disks. These models are quite effective at suggesting sizes and masses of the disks but, unfortunately, are unable to select an appropriate density gradient, given the inherent inaccuracies in the calibration of submillimeter data. Masses derived from these models indicate disk masses of a few thousandths to a few tenths of a solar mass (in gas plus dust, assuming a ratio of 100:1 of gas to dust, by mass) are common, but they suggest that disk sizes may range from tens to a few thousand of AU. The large ranges in the mass estimates are due primarily to our inability to place observational constraints on the density index. For many of the HBes, for which the emission is extended so that we can probably safely assume the dust is nearly isothermal and optically thin, we find nebula masses ranging from several (LkH-α 234, MWC 1080) to many tens (V645 Cyg) of solar masses. Models for the FUors indicate that they have shallower temperature gradients (temperature ∝ radius$^{-0.44 \text{ to } -0.54}$) than cTTs. This result suggests that these disks may be active, i.e. that the outer parts of the disks generate additional heat from active accretion of additional mass from the remnant cloud.

Five-point 800 μm maps and diffraction limited 450 μm maps

By measuring the sizes of several sources at 800 and 450 μm, we have found that thermal emission sources around many pre-main-sequence stars are extended (Weintraub, Sandell and Duncan 1990, 1991b; Sandell, Weintraub and Duncan 1991). These maps demonstrate that at least some of the emission may arise from dust swept up into outflowing jets or from remnant structures no longer associated with the stars' or the disks' evolution. At 800 μm, the FUors Elias 1-12 (deconvolved FWHM = 17"x28" using a 16" beam; d=900 pc) and V346 Nor (37"x12"; 620 pc), the HBes LkH-α 198 (14"x11"), V645 Cyg (17"x14"; 5.6 kpc), LkH-α 234 (8"x7"; 1.25kpc) and MWC 1080 (~15"; 2.2 kpc) and the cTTs T Tauri (11"x11") and HL Tauri (7.5"x7.5") were all resolved. The higher resolution maps at 450 μm suggest that not all of the 450 μm emission from some stars emerges from compact (<7" FWHM) cores that might be attributed to circumstellar disks. Around LkH-α 234 the remaining flux emerges from jetlike features and from a ridge of emission (Figure 1). A small amount of flux also is associated with fingers of emission in maps of HL Tauri and PP 13. In a case like LkH-α 234, although it is associated with extended emission, we can use the results from our mapping to obtain much more accurate flux estimates of the compact

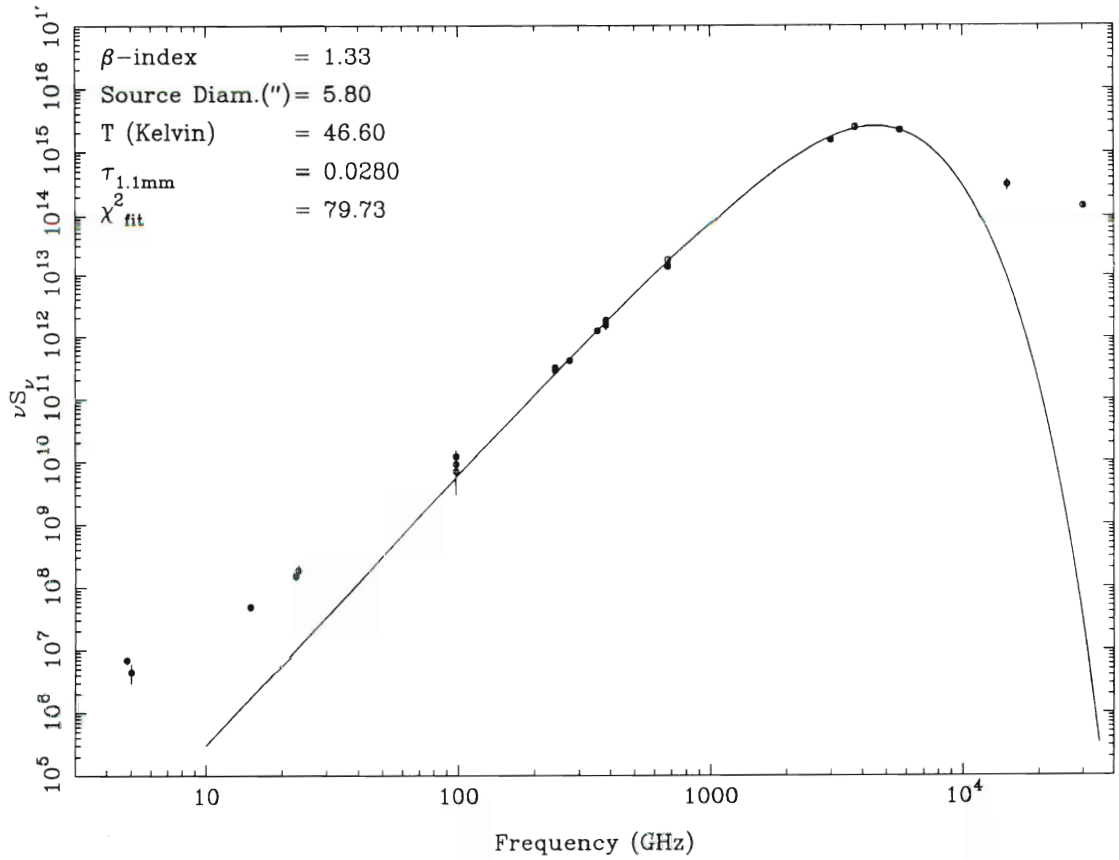

Figure 2. The spectral energy distribution of the compact emission from LkH-α 234. The plot includes the free-free emission seen at cm-wavelengths, as well as FIR data from KAO and groundbased mid-infrared data. One can see that the sub-mm & FIR data points are well fitted by an isothermal dust cloud model, constrained to the measured 450 μm size of the source (solid curve). The mass derived from this isothermal dust fit is ~ 1.2 $M_\odot$, while an equally good fit using a disk model predicts the mass to be < ~ 0.4 $M_\odot$. The isothermal model fit predicts gas densities of 8 $10^5 cm^{-3}$ and a line of sight visual extinction of 44 mag, clearly a contradiction, since the measured extinction is only 3 mag. Therefore it is much more plausible to assume that the emission originates from a disk, rather than a spherical envelope.

emission surrounding the stars. The spectral energy distribution of LkH-α 234 (Figure 2), derived from both photometry and mapping, clearly illustrates the power of this technique.

Conclusions

Our results raise questions about the normal method of analysis and interpretation of large aperture, single passband, sub-mm continuum data. For many sources, the canonical model (an optically thin, 100 AU disk; dust grain opacity characterized by $1 < \beta < 2$) may not apply. We have found that many pre-main-sequences are optically thick through much of the sub-mm and mm regime, that the emission source is resolved at 450 and/or 800 μm, indicating sizes of order many 1000s of AU, that the morphology of some of the extended sources suggests that the dust is associated with outflows and with large structures that may be remnants of the protostellar cloud that have little or nothing to do with preplanetary disks, and finally that the effective β index is often between 0 and 1, rather than between 1 and 2.

David Weintraub and Goeran Sandell
JAC

References

Adams, F., Lada, C. and Shu, F. 1988, Ap.J., 357, 606.
Casey, S.C. and Harper, D.A. 1990, Ap.J., 362, 663.
Hartmann, L. et al. 1989, Ap.J. 338, 1001.
Sandell, G., Weintraub, D.A. and Duncan, W.D. 1991, in preparation.
Weintraub, D.A. 1990, Ap.J.Suppl., 74, 575.
Weintraub, D.A., Sandell, G. and Duncan, W.D. 1989, Ap.J.Lett., 340, L69.
Weintraub, D.A., Sandell, G. and Duncan, W.D. 1991a, Ap.J., submitted.
Weintraub, D.A., Sandell, G. and Duncan, W.D. 1991b, Bull.A.A.S, 20, 1265..

Points of Contact

Joint Astronomy Centre
665 Komohana Street
Hilo
Hawaii 96720
USA

Telephone numbers:
Prefix from outside Hawaii 1 808
Prefix from UK 010 1 808

JAC
Phone: 961 3756
935 4332 (answerphone)
Telex: 633135 on WUI
Fax: 961 6516
e-mail: PSS: 315280809053
STARLINK: JACH
Span: 19527::JACH
Internet: JACH.HAWAII.EDU
(from Janet
CBS%NSFNET-RELAY::EDU.HAWAII.JACH)

Mauna Kea

JAC Offices at Hale Pohaku 935 9911
JCMT Carousel: 935 0852
UKIRT dome: 961 6091
Fax in JCMT carousel: 935 5493

Royal Observatory Edinburgh
Blackford Hill
Edinburgh EH9 3HJ
UK

Telephone:
From outside UK, omit 0 & prefix by 44
ROE has a telephone system which allows extension numbers to be dialled by the caller.

Switchboard: 031 668 8100

JCMT Section:
Dorothy Skedd 031 668 8306

UKIRT Section:
Maureen McLean 031 668 8309
(and answerphone after hours)

Fax: 031 668 8264
e-mail: UK.AC.ROE.STAR
Starlink: REVAD

Starlink Directories:
JCMT REVAD::DISK$USER3:[JCMT]
UKIRT Vaxnotes on RESTAR::UKIRT
or UKIRTINFORM

The Newsletter is distributed in Canada by the HIA, Ottawa. Readers in Canada wishing to be placed on the mailing list should contact:

Dr John McLeod
Herzberg Institute of Astrophysics
100 Sussex Drive
Ottawa
Ontario K1A 0R6
Canada

User manuals

User manuals, recently updated, are being sent to libraries. Copies may be obtained by contacting:
Henry Matthews at JAC (JCMT)
Dorothy Skedd at ROE (JCMT)
Maureen McLean at ROE (UKIRT)

Editor of Newsletter:

Liz Sim 031 668 8315
MES on REVAD

Please send material for the next edition of this Newsletter to the Editor by December 1 1991 - earlier if possible, please.

ISSN 0963-2700